Available online at www.sciencedirect.com
ScienceDirect
Journal of Solid State Chemistry 180 (2007) 1720–1736
JOURNAL OF SOLID STATE CHEMISTRY
www.elsevier.com/locate/jssc

Rare earth–transition metal–magnesium compounds—An overview

Ute Ch. Rodewald[a], Bernard Chevalier[b], Rainer Pöttgen[a,*]

[a]*Institut für Anorganische und Analytische Chemie, Universität Münster, Corrensstrasse 30, D-48149 Münster, Germany*
[b]*Institut de Chimie de la Matière Condensée de Bordeaux (ICMCB), CNRS [UPR 9048], Université Bordeaux 1, 87 avenue du Docteur Albert Schweitzer, F-33608 Pessac Cedex, France*

Received 9 January 2007; received in revised form 28 February 2007; accepted 5 March 2007
Available online 12 March 2007

Abstract

Intermetallic rare earth–transition metal–magnesium compounds play an important role as precipitations in modern light weight alloys and as host materials for hydrogen storage applications. Recent results on the crystal chemistry, the chemical bonding peculiarities, physical properties, and hydrogenation behavior of these materials are reviewed.
© 2007 Elsevier Inc. All rights reserved.

Keywords: Magnesium; Intermetallics; Crystal chemistry

1. Introduction

Intermetallic magnesium compounds gain significant technical importance for precipitation hardening (optimization of the microstructure and the mechanical properties) [1–3, and references therein] in modern light weight alloys or for hydrogen storage applications [4–8].

In that view, the ternary systems rare earth metal (*RE*)–transition metal (*T*)–magnesium have intensively been studied in the last ten years with respect to phase analyses, crystal chemistry, physical properties, and hydrogenation behavior. The recent developments are summarized herein. This short review is written from a solid state chemist's point of view with an emphasis on crystalline materials and structural chemistry.

2. Synthesis techniques

The rare earth–transition metal–magnesium compounds can be prepared directly from the pure elements. Especially the air sensitive early rare earth elements, including europium [9], need careful handling in order to avoid surface oxidation and/or hydrolysis. Magnesium can be used in the form of rods. The surface needs first to be cut on a turning lathe in order to remove surface impurities (the ceramic MgO with huge lattice energy may act as a thermodynamic trap). Due to the low boiling temperature (1363 K [10]) of magnesium, synthesis in a quasi-open system (arc-melting furnace) is not possible, since significant evaporations would irreversibly affect the synthesis.

An effective way is the synthesis of such $RE_xT_yMg_z$ intermetallic compounds in inert, high-melting metal ampoules made of niobium or tantalum [11,12]. These container materials show no reaction with the melt. The reactions can be carried out in a water-cooled sample chamber of an induction furnace [13,14] and the approximate reaction temperatures can be monitored through a pyrometer. Some authors also used silver ampoules for the synthesis [15]. The $RE_xT_yMg_z$ intermetallic compounds can easily be obtained in amounts of 1–2 g via this synthesis technique. The light gray polycrystalline samples are quite brittle and stable in air. Finely ground powders are dark gray; single crystals exhibit metallic luster.

Besides the classical reactions through a melt, such compounds are also accessible via ball-milling [16–18]. Amorphous and nanocrystalline magnesium-based alloys and intermetallics can be obtained by rapid solidification through melt-spinning [19,20].

Several authors used simple sintering reactions of cold-pressed pellets of the elemental mixtures [21,22]. Typical

*Corresponding author. Fax: +49 251 83 36002.
E-mail addresses: chevalie@icmcb-bordeaux.cnrs.fr (B. Chevalier), pottgen@uni-muenster.de (R. Pöttgen).

0022-4596/$ - see front matter © 2007 Elsevier Inc. All rights reserved.
doi:10.1016/j.jssc.2007.03.007

annealing sequences are RT → 673 K → 923 K → 973 K → RT. These techniques are problematic, since mostly no liquid phase (or a complete melt) is present and not all phases form under these conditions. To give an example, study of the Y–Ni–Mg [23], Ce–Ni–Mg [24], and Pr–Ni–Mg [25] phase diagrams via sintered pellets did not reveal Y_2Ni_2Mg, Ce_2Ni_2Mg, and Pr_2Ni_2Mg obtained directly from the melt in sealed tantalum tubes [26].

3. Crystal chemistry and chemical bonding

The many $RE_xT_yMg_z$ compounds crystallize in few, relatively simple structure types. The basic crystallographic data are listed in Table 1. In the following subsections we discuss the different structure types. The positional parameters for one representative compound of each structure type are listed in Table 2.

3.1. The structure types Mo_2FeB_2 and $Nd_4Co_2Mg_3$

More than 30 intermetallic RE_2T_2Mg compounds (T = late transition metal) crystallize with the tetragonal Mo_2FeB_2 type structure [62], space group $P4/mbm$. As an example we present the Ce_2Cu_2Mg structure [27] in Fig. 1. The structure can be considered as a simple 1:1 intergrowth of AlB_2 and CsCl-related slabs of compositions $CeCu_2$ and CeMg. The copper atoms form Cu_2 dumb-bells at Cu–Cu distances of 268 pm, slightly longer than the Cu–Cu distance of 256 pm in fcc copper [63]. Always four Cu_2 dumb-bells coordinate to a magnesium atom at Cu–Mg of 314 pm, significantly longer than the sum of the covalent radii of 253 pm [10].

It is interesting to note, that also several series of isotypic RE_2T_2In indides exists [65]. Extended-Hückel band structure calculations for La_2Cu_2In and La_2Cu_2Mg [29] revealed weaker Cu–Mg interactions as compared to Cu–In in the indide. The same was observed for La–In vs. La–Mg. The course of the a and c lattice parameters is thus governed by different factors. The strength of the T–Mg and T–In interactions strongly influences the a parameter, while the lattice parameter c more or less depends on the nature (size; lanthanoid contraction) of the rare earth element. For that reason, the a parameters of the indide series are smaller than those of the respective magnesium series, while the c parameters are almost similar. For an overview on the family of Mo_2FeB_2 type intermetallics we refer to a recent review [65].

For Ce_2Pd_2Mg and Nd_2Pd_2Mg a small range of homogeneity $Ce_2Pd_{2+x}Mg_{1-x}$ has been detected on the basis of single crystal X-ray data [27,35]. Refinement of the occupancy parameters revealed higher electron density for the magnesium position within the CsCl slab. The highest palladium content has been observed for $Ce_2Pd_{2.07}Mg_{0.93}$ and $Nd_2Pd_{2.11}Mg_{0.89}$. This behavior is similar to the antiferromagnetic stannide $Ce_2Pd_{2+x}Sn_{1-x}$ ($0.04 \leqslant x \leqslant 0.21$) [66].

The Mo_2FeB_2 type structure occurs for the RE_2Ni_2Mg [26] and the RE_2Cu_2Mg [29] series, but no cobalt-based analogs have been observed. Instead we observed another intergrowth structure, the $Nd_4Co_2Mg_3$ type [38], space group $P2/m$, which can be considered as a 1:3 intergrowth variant of distorted AlB_2 and CsCl related slabs of compositions $NdCo_2$ and NdMg. This monoclinic structure type is formed also with RE = Pr, Sm, Gd, Tb, and Dy [40]. The Co_2 dumb-bells in the neodymium compound have Co–Co distances of 237 pm, somewhat shorter than the average Co–Co distance of 250 pm in *hcp* cobalt [63]. The rectangular faces of the trigonal prisms are capped by one cobalt atom (from the Co_2 dumb-bell) and two magnesium atoms, leading to coordination number (CN) 9, typically observed for the transition metal atoms in this and related structures. The Mg–Mg distances of 317 pm are even smaller than the average Mg–Mg distance of 320 pm in *hcp* magnesium [63], however, the shorter distances are a geometrical constraint of the distortion of the REMg and $RECo_2$ slabs.

Besides Co–Co, the shortest interatomic distances in the $Nd_4Co_2Mg_3$ structure occur between the neodymium and cobalt atoms, i.e. 275 pm Co–Nd2 (2 ×), 294 pm Co–Nd1 (2 ×), and 299 pm Co–Nd1 (2 ×). All these Co–Nd distances are close to the sum of the covalent radii of 280 pm, and we can safely assume strong Co–Nd bonding. This was underlined by recent electronic structure calculations [40].

3.2. The structure types ZrNiAl, TiNiSi and LaNiAl

A huge number of equiatomic RETMg compounds (Table 1) has been observed with rhodium, palladium, silver, platinum, and gold as transition metal component. Those RETMg compounds with a stable trivalent rare earth element crystallize with the hexagonal ZrNiAl [67–69] type, space group $P\bar{6}2m$. As an example we present the PrAuMg structure [28] in Fig. 2. The two crystallographically independent gold sites have different trigonal prismatic coordination, i.e. $[Au1Pr_6Mg_3]$ and $[Au2Mg_6Pr_3]$. Both types of trigonal prisms are condensed via the triangular faces in the c direction. The Au1 centered prisms build up larger ring units of six prisms around the rows of the Au2 centered prisms. The shortest interatomic distances occur between the gold and magnesium atoms which build up a three-dimensional [AuMg] network in which the praseodymium atoms fill distorted hexagonal channels. The crystal chemistry of the many ZrNiAl type intermetallic compounds has repeatedly been reviewed. For more details we refer to this literature [70,71].

X-ray powder data have been reported for the nickel based compounds LaNiMg and CeNiMg [53]. The patterns revealed weak superstructure reflections pointing to the orthorhombic TiFeSi type [72], a superstructure of ZrNiAl. However, precise positional parameters of these compounds are not available.

Table 1
Lattice parameters, space groups and structure types of the intermetallic rare earth–transition metal–magnesium compounds

Compound	Type	SG	a (pm)	b (pm)	c (pm)	V (nm^3)	Ref.
Y_4CoMg	Gd_4RhIn	$F\bar{4}3m$	1364.3(4)	a	a	2.5393	[39]
YNi_9Mg_2	$PuNi_3$	$R\bar{3}m$	486.66(5)	a	2377.33(5)	0.4876	[49]
YNi_4Mg	$MgCu_4Sn$	$F\bar{4}3m$	718.53(3)	a	a	0.3710	[22]
YNi_4Mg	$MgCu_4Sn$	$F\bar{4}3m$	701	a	a	0.3445	[59,64]
Y_2Ni_2Mg	Mo_2FeB_2	$P4/mbm$	740.5(1)	a	372.5(1)	0.2043	[26]
$Y_2Ni_{1.90}Mg$[a]	Mo_2FeB_2	$P4/mbm$	740.4(1)	a	372.3(1)	0.2041	[26]
YCu_9Mg_2	$TbCu_9Mg_2$	$P6_3/mmc$	500.44(2)	a	1620.31(9)	0.3514	[42]
Y_2Cu_2Mg	Mo_2FeB_2	$P4/mbm$	762.65(5)	a	374.09(3)	0.2176	[29]
Y_4RhMg	Gd_4RhIn	$F\bar{4}3m$	1377.0(2)	a	a	2.6109	[44]
Y_2Pd_2Mg	Mo_2FeB_2	$P4/mbm$	764.6(2)	a	378.0(1)	0.2210	[35]
YPdMg	ZrNiAl	$P\bar{6}2m$	743.0(1)	a	405.4(1)	0.1938	[41]
YAgMg	ZrNiAl	$P\bar{6}2m$	766.1(2)	a	413.8(1)	0.2103	[41]
YAuMg	ZrNiAl	$P\bar{6}2m$	752.3(2)	a	409.4(1)	0.2007	[28]
La_4CoMg	Gd_4RhIn	$F\bar{4}3m$	1428.38(9)	a	a	2.9143	[39]
$LaNi_9Mg_2$	$PuNi_3$	$R\bar{3}m$	492.35(3)	a	2386.6(3)	0.5010	[21]
$LaNi_9Mg_2$	$PuNi_3$	$R\bar{3}m$	492.41(14)	a	2387.5(3)	0.5013	[52]
$LaNi_9Mg_2$	$PuNi_3$	$R\bar{3}m$	488.6(3)	a	2398(1)	0.4958	[60]
$LaNi_4Mg$	$MgCu_4Sn$	$F\bar{4}3m$	717.94(2)	a	a	0.3700	[22]
$LaNi_4Mg$	$MgCu_4Sn$	$F\bar{4}3m$	730.2(3)	a	a		[60]
La_2Ni_2Mg	Mo_2FeB_2	$P4/mbm$	764.5(1)	a	394.39(9)	0.2305	[26]
La_2Ni_2Mg[a]	Mo_2FeB_2	$P4/mbm$	765.4(1)	a	392.6(1)	0.2300	[26]
$La_2Ni_3Mg_3$	$Sm_2Zn_3Mg_3$	fcc	703.6	a	a	0.3483	[53]
LaNiMg	TiFeSi	$Ima2$	864	1333	745	0.8580	[53]
$LaNiMg_2$	$MgCuAl_2$	$Cmcm$	422.66(6)	1030.3(1)	836.0(1)	0.3640	[45]
$LaNiMg_2$	$MgCuAl_2$	$Cmcm$	416	1065	782	0.3465	[53]
$LaNiMg_2$	$MgCuAl_2$	$Cmcm$	422.1(1)	1027.5(2)	835.4(1)	0.3623	[61]
$LaCu_9Mg_2$	$TbCu_9Mg_2$	$P6_3/mmc$	507.33(2)	a	1626.33(9)	0.3625	[42]
$LaCu_9Mg_2$	$TbCu_9Mg_2$	$P6_3/mmc$	507.34(2)	a	1626.3(9)	0.3625	[56]
La_2Cu_2Mg	Mo_2FeB_2	$P4/mbm$	792.09(6)	a	396.31(8)	0.2486	[29]
La_2Cu_2Mg	Mo_2FeB_2	$P4/mbm$	791.9(1)	a	397.0(1)	0.2490	[48]
$LaCu_2Mg$	$ZrPt_2Al$	$P6_3/mmc$	467.05(1)	a	887.26(4)	0.1676	[56]
LaCuMg	ZrNiAl	$P\bar{6}2m$	772.5(3)	a	418.8(2)	0.2164	[50]
LaCuMg	ZrNiAl	$P\bar{6}2m$	773.2(5)	a	417.9(1)	0.2164	[56]
$LaCu_2Mg_2$	?	hexagonal	518.62(5)	a	1979.9(4)	0.4612	[51]
$LaCuMg_2$	BiF_3	$Fm\bar{3}m$	730.2(8)	a	a	0.3893	[56]
$LaCuMg_4$	?	tetragonal	901.5(1)	a	519.9(1)	0.4225	[56]
La_4RhMg	Gd_4RhIn	$F\bar{4}3m$	1437.1(1)	a	a	2.9679	[44]
LaRhMg	LaNiAl	$Pnma$	760.1(2)	419.92(8)	1702.6(2)	0.5434	[32]
La_2Pd_2Mg	Mo_2FeB_2	$P4/mbm$	782.1(2)	a	407.5(2)	0.2493	[48]
LaPdMg	ZrNiAl	$P\bar{6}2m$	771.8(1)	a	414.1(1)	0.2136	[41]
LaPdMg	ZrNiAl	$P\bar{6}2m$	773.6(1)	a	413.79(4)	0.2145	[33]
LaAgMg	ZrNiAl	$P\bar{6}2m$	788.8(3)	a	437.4(1)	0.2357	[30]
LaAgMg	ZrNiAl	$P\bar{6}2m$	785.3(2)	a	437.0(2)	0.2334	[41]
LaPtMg	ZrNiAl	$P\bar{6}2m$	762.0(1)	a	417.48(5)	0.2099	[33]
LaAuMg	ZrNiAl	$P\bar{6}2m$	781.0(1)	a	425.49(9)	0.2248	[33]

$Ce_2Fe_2Mg_{15}$	$Ce_2Fe_2Mg_{15}$	$P6_3/mmc$	1032.4(5)	*a*	1028.0(4)	0.9489	[55]
$CeNi_9Mg_2$	$PuNi_3$	$R\bar{3}m$	487.06(6)	*a*	2384.6(3)	0.4899	[21]
$CeNi_4Mg$	$MgCu_4Sn$	$F\bar{4}3m$	703.73(4)	*a*	*a*	0.3485	[22]
$CeNi_4Mg$	$MgCu_4Sn$	$F\bar{4}3m$	700	*a*	*a*	0.3430	[47]
$Ce_2Ni_3Mg_3$	$Sm_2Zn_3Mg_3$	*fcc*	701.9	*a*	*a*	0.3458	[53]
Ce_2NiMg_3	?	cubic	707.6	*a*	*a*	0.3543	[53]
Ce_2Ni_2Mg	Mo_2FeB_2	$P4/mbm$	759.6(1)	*a*	376.71(9)	0.2174	[27]
Ce_2Ni_2Mg	Mo_2FeB_2	$P4/mbm$	757	*a*	376	0.2155	[47]
CeNiMg	TiFeSi	*Ima*2	854	1310	736	0.8234	[53]
$CeCu_9Mg_2$[a]	$TbCu_9Mg_2$	$P6_3/mmc$	506.1	*a*	1626.0	0.3606	[42]
$CeCu_9Mg_2$	$TbCu_9Mg_2$	$P6_3/mmc$	505.58(2)	*a*	1624.39(10)	0.3596	[42]
$CeCu_2Mg$	$ZrPt_2Al$	$P6_3/mmc$	465.7(1)	*a*	865.4(3)	0.1625	[46]
Ce_2Cu_2Mg	Mo_2FeB_2	$P4/mbm$	787.41(9)	*a*	387.23(7)	0.2401	[27]
Ce_2Cu_2Mg	Mo_2FeB_2	$P4/mbm$	786.8(1)	*a*	387.5(2)	0.2399	[29]
Ce_2Cu_2Mg	Mo_2FeB_2	$P4/mbm$	787.41(9)	*a*	387.23(2)	0.2399	[48]
CeCuMg	ZrNiAl	$P\bar{6}2m$	766.8(5)	*a*	416.4(4)	0.2120	[50]
Ce_4RhMg	Gd_4RhIn	$F\bar{4}3m$	1417.5(1)	*a*	*a*	2.8484	[44]
$CeRh_{1.262}Mg_{0.738}$	ZrNiAl	$P\bar{6}2m$	752.3(1)	*a*	417.6(1)	0.2047	[32]
Ce_2Pd_2Mg	Mo_2FeB_2	$P4/mbm$	777.14(8)	*a*	400.03(7)	0.2416	[27]
CePdMg	ZrNiAl	$P\bar{6}2m$	765.1(1)	*a*	410.3(1)	0.2080	[41]
CePdMg	ZrNiAl	$P\bar{6}2m$	760	*a*	408	0.2041	[47]
CePdMg	ZrNiAl	$P\bar{6}2m$	767.3(1)	*a*	410.37(4)	0.2092	[33]
CeAgMg	ZrNiAl	$P\bar{6}2m$	782.5(3)	*a*	432.8(1)	0.2295	[30]
CeAgMg	ZrNiAl	$P\bar{6}2m$	782.3(2)	*a*	433.1(1)	0.2295	[41]
CePtMg	ZrNiAl	$P\bar{6}2m$	755.02(7)	*a*	413.82(4)	0.2043	[33]
CeAuMg	ZrNiAl	$P\bar{6}2m$	774.1(3)	*a*	421.6(1)	0.2188	[28]
$CeAuIn_{0.871}Mg_{0.129}$[a]	ZrNiAl	$P\bar{6}2m$	774.54(7)	*a*	420.32(10)	0.2184	[37]
$CeAuIn_{0.8}Mg_{0.2}$	ZrNiAl	$P\bar{6}2m$	775.0(1)	*a*	420.51(5)	0.2187	[37]
$CeAuIn_{0.640}Mg_{0.360}$[a]	ZrNiAl	$P\bar{6}2m$	775.25(7)	*a*	419.36(10)	0.2183	[37]
$CeAuIn_{0.6}Mg_{0.4}$	ZrNiAl	$P\bar{6}2m$	776.3(1)	*a*	419.87(6)	0.2192	[37]
$CeAuIn_{0.445}Mg_{0.555}$[a]	ZrNiAl	$P\bar{6}2m$	774.62(7)	*a*	420.13(10)	0.2183	[37]
$CeAuIn_{0.4}Mg_{0.6}$	ZrNiAl	$P\bar{6}2m$	776.0(1)	*a*	420.52(5)	0.2193	[37]
$CeAuIn_{0.228}Mg_{0.772}$[a]	ZrNiAl	$P\bar{6}2m$	773.80(11)	*a*	420.82(8)	0.2182	[37]
$CeAuIn_{0.2}Mg_{0.8}$[a]	ZrNiAl	$P\bar{6}2m$	774.8(1)	*a*	421.27(7)	0.2190	[37]
Pr_4CoMg	Gd_4RhIn	$F\bar{4}3m$	1399.5(2)	*a*	*a*	2.7408	[39]
$Pr_4Co_2Mg_3$	$Nd_4Co_2Mg_3$	$P2/m$	771.8(3)	383.9(2)	840.5(4) $\beta = 109.90(5)^\circ$	0.2342	[40]
$PrNi_9Mg_2$	$PuNi_3$	$R\bar{3}m$	488.68(4)	*a*	2385.4(3)	0.4933	[21]
$PrNi_4Mg$	$MgCu_4Sn$	$F\bar{4}3m$	712.37(6)	*a*	*a*	0.3615	[22]
Pr_2Ni_2Mg	Mo_2FeB_2	$P4/mbm$	754.4(1)	*a*	385.20(9)	0.2192	[26]
Pr_2Ni_2Mg[a]	Mo_2FeB_2	$P4/mbm$	754.9(1)	*a*	384.1(1)	0.2189	[26]
$PrCu_9Mg_2$	$TbCu_9Mg_2$	$P6_3/mmc$	504.69(3)	*a*	1623.60(11)	0.3582	[42]
Pr_2Cu_2Mg	Mo_2FeB_2	$P4/mbm$	782.82(8)	*a*	385.12(6)	0.2360	[29]
Pr_4RhMg	Gd_4RhIn	$F\bar{4}3m$	1415.1(5)	*a*	*a*	2.8335	[44]
PrRhMg	TiNiSi	*Pnma*	721.62(7)	415.98(4)	869.47(8)	0.2610	[32]
Pr_2Pd_2Mg	Mo_2FeB_2	$P4/mbm$	775.3(2)	*a*	396.8(1)	0.2385	[35]
PrPdMg	ZrNiAl	$P\bar{6}2m$	763.6(2)	*a*	408.5(1)	0.2063	[41]
PrAgMg	ZrNiAl	$P\bar{6}2m$	779.7(3)	*a*	429.3(3)	0.2260	[41]
PrPtMg	ZrNiAl	$P\bar{6}2m$	752.34(8)	*a*	412.66(4)	0.2023	[31]
PrAuMg	ZrNiAl	$P\bar{6}2m$	770.8(2)	*a*	419.5(1)	0.2158	[28]

Table 1 (*continued*)

Compound	Type	SG	*a* (pm)	*b* (pm)	*c* (pm)	*V* (nm^3)	Ref.
$Nd_{3.90}CoMg_{1.10}$	Gd_4RhIn	$F\bar{4}3m$	1390.2(3)	*a*	*a*	2.6866	[39]
$Nd_4Co_2Mg_3$	$Nd_4Co_2Mg_3$	$P2/m$	765.42(14)	380.53(5)	832.47(16) $\beta = 109.79(1)^\circ$	0.2282	[38]
$NdNi_9Mg_2$	$PuNi_3$	$R\bar{3}m$	489.60(6)	*a*	2384.2(5)	0.4949	[21]
$NdNi_4Mg$	$MgCu_4Sn$	$F\bar{4}3m$	712.34(4)	*a*	*a*	0.3615	[22]
$NdNi_4Mg$	$MgCu_4Sn$	$F\bar{4}3m$	709.875(1)	*a*	*a*	0.3577	[15]
Nd_2Ni_2Mg[a]	Mo_2FeB_2	$P4/mbm$	753.3(1)	*a*	381.8(1)	0.2167	[26]
Nd_2Ni_2Mg	Mo_2FeB_2	$P4/mbm$	752.53(8)	*a*	382.33(5)	0.2165	[26]
$Nd_{0.05}NiMg_{1.95}$	Mg_2Ni	$P6_222$	523.1	*a*	1330.3	0.3152	[57]
$Nd_{0.1}NiMg_{1.9}$	Mg_2Ni	$P6_222$	523.7	*a*	1331.7	0.3163	[57]
$Nd_{0.2}NiMg_{1.8}$	Mg_2Ni	$P6_222$	524.9	*a*	1334.7	0.3185	[57]
$NdCu_9Mg_2$	$TbCu_9Mg_2$	$P6_3/mmc$	504.30(3)	*a*	1624.50(10)	0.3578	[42]
Nd_2Cu_2Mg	Mo_2FeB_2	$P4/mbm$	778.30(5)	*a*	384.04(5)	0.2326	[29]
Nd_4RhMg	Gd_4RhIn	$F\bar{4}3m$	1405.9(2)	*a*	*a*	2.7786	[44]
NdRhMg	TiNiSi	*Pnma*	720.6(1)	417.6(1)	868.8(1)	0.2615	[32]
Nd_2Pd_2Mg	Mo_2FeB_2	$P4/mbm$	774.4(2)	*a*	393.37(8)	0.2359	[35]
NdPdMg	ZrNiAl	$P\bar{6}2m$	763.2(2)	*a*	408.3(1)	0.2060	[35]
NdAgMg	ZrNiAl	$P\bar{6}2m$	775.7(3)	*a*	426.1(1)	0.2220	[30]
NdPtMg	ZrNiAl	$P\bar{6}2m$	748.80(8)	*a*	411.52(4)	0.1998	[31]
NdAuMg	ZrNiAl	$P\bar{6}2m$	767.2(2)	*a*	418.1(1)	0.2131	[28]
$Sm_{3.92}Co_{0.93}Mg_{1.08}$	Gd_4RhIn	$F\bar{4}3m$	1381.0(3)	*a*	*a*	2.6335	[39]
$Sm_4Co_2Mg_3$	$Nd_4Co_2Mg_3$	$P2/m$	760.12(15)	377.11(6)	826.84(16) $\beta = 109.68(1)$	0.2232	[38]
$SmNi_9Mg_2$	$PuNi_3$	$R\bar{3}m$	488.78(4)	*a*	2378.5(4)	0.4921	[21]
Sm_2Ni_2Mg	Mo_2FeB_2	$P4/mbm$	746.02(9)	*a*	379.34(8)	0.2111	[26]
$SmCu_9Mg_2$	$TbCu_9Mg_2$	$P6_3/mmc$	502.70(2)	*a*	1622.04(10)	0.3550	[42]
Sm_2Cu_2Mg	Mo_2FeB_2	$P4/mbm$	771.45(6)	*a*	379.52(5)	0.2259	[29]
$Sm_2Zn_3Mg_3$	$CaMg_3Zn_6$	?	1462	*a*	878	1.8767	[54]
Sm_4RhMg	Gd_4RhIn	$F\bar{4}3m$	1392.1(1)	*a*	*a*	2.6979	[44]
Sm_2Pd_2Mg	Mo_2FeB_2	$P4/mbm$	770.38(8)	*a*	388.29(7)	0.2304	[35]
SmPdMg	ZrNiAl	$P\bar{6}2m$	755.4(1)	*a*	405.0(1)	0.2001	[41]
SmAgMg	ZrNiAl	$P\bar{6}2m$	773.0(1)	*a*	422.4(1)	0.2186	[41]
SmPtMg	ZrNiAl	$P\bar{6}2m$	743.90(5)	*a*	409.80(3)	0.1964	[31]
SmAuMg	ZrNiAl	$P\bar{6}2m$	761.91(9)	*a*	414.98(7)	0.2086	[28]
$EuCu_9Mg_2$	$TbCu_9Mg_2$	$P6_3/mmc$	506.93(2)	*a*	1622.72(10)	0.3611	[42]
EuPdMg	TiNiSi	*Pnma*	753.85(9)	440.27(4)	866.27(9)	0.2875	[35]
EuAgMg	TiNiSi	*Pnma*	777.4(2)	463.0(1)	898.8(2)	0.3235	[30]
EuAuMg	TiNiSi	*Pnma*	760.6(3)	448.8(2)	875.8(2)	0.2990	[28]
$Gd_{3.92}CoMg_{1.08}$	Gd_4RhIn	$F\bar{4}3m$	1373.1(4)	*a*	*a*	2.5887	[39]
$Gd_4Co_2Mg_3$	$Nd_4Co_2Mg_3$	$P2/m$	754.0(4)	374.1(1)	822.5(3) $\beta = 109.65(4)^\circ$	0.2185	[40]
$GdNi_9Mg_2$	$PuNi_3$	$R\bar{3}m$	487.31(3)	*a*	2376.6(2)	0.4888	[21]
Gd_2Ni_2Mg	Mo_2FeB_2	$P4/mbm$	743.8(1)	*a*	375.3(1)	0.2076	[26]
$GdCu_9Mg_2$	$TbCu_9Mg_2$	$P6_3/mmc$	501.64(3)	*a*	1621.63(12)	0.3534	[42]
Gd_2Cu_2Mg	Mo_2FeB_2	$P4/mbm$	765.31(8)	*a*	377.22(7)	0.2209	[29]
Gd_4RhMg	Gd_4RhIn	$F\bar{4}3m$	1380.8(2)	*a*	*a*	2.6328	[44]

Gd_2Pd_2Mg	Mo_2FeB_2	$P4/mbm$	767.9(1)	a	383.9(1)	0.2264	[35]
GdPdMg	ZrNiAl	$P\bar{6}2m$	750.2(1)	a	404.2(1)	0.1970	[41]
GdPdMg	ZrNiAl	$P\bar{6}2m$	750.1(1)	a	404.10(4)	0.1969	[34]
GdAgMg	ZrNiAl	$P\bar{6}2m$	768.0(2)	a	419.92(9)	0.2145	[34]
GdAgMg	ZrNiAl	$P\bar{6}2m$	767.9(2)	a	419.9(1)	0.2144	[30]
GdAgMg	ZrNiAl	$P\bar{6}2m$	767.9(1)	a	418.9(1)	0.2139	[41]
GdPtMg	ZrNiAl	$P\bar{6}2m$	738.0(1)	a	409.02(5)	0.1929	[34]
GdAuMg	ZrNiAl	$P\bar{6}2m$	756.7(1)	a	413.09(5)	0.2048	[28]
GdAuMg	ZrNiAl	$P\bar{6}2m$	756.3(1)	a	412.71(5)	0.2044	[36]
$Tb_{3.77}CoMg_{1.23}$	Gd_4RhIn	$F\bar{4}3m$	1362.1(3)	a	a	2.5271	[39]
$Tb_4Co_2Mg_3$	$Nd_4Co_2Mg_3$	$P2/m$	750.4(2)	372.86(6)	819.5(2) $\beta = 109.48(3)^\circ$	0.2162	[40]
Tb_2Ni_2Mg	Mo_2FeB_2	$P4/mbm$	740.4(1)	a	372.66(8)	0.2043	[26]
$TbCu_9Mg_2$[a]	$TbCu_9Mg_2$	$P6_3/mmc$	498.86(15)	a	1616.5(5)	0.3485	[42]
$TbCu_9Mg_2$	$TbCu_9Mg_2$	$P6_3/mmc$	500.85(4)	a	1620.60(15)	0.3521	[42]
Tb_2Cu_2Mg	Mo_2FeB_2	$P4/mbm$	762.57(9)	a	373.94(9)	0.2175	[29]
Tb_4RhMg	Gd_4RhIn	$F\bar{4}3m$	1370.7(2)	a	a	2.5751	[44]
Tb_2Pd_2Mg	Mo_2FeB_2	$P4/mbm$	762.56(8)	a	380.55(7)	0.2213	[35]
TbPdMg	ZrNiAl	$P\bar{6}2m$	746.40(8)	a	403.05(4)	0.1945	[35]
TbAgMg	ZrNiAl	$P\bar{6}2m$	763.9(3)	a	416.5(1)	0.2105	[30]
TbAuMg	ZrNiAl	$P\bar{6}2m$	754.6(1)	a	410.82(6)	0.2026	[28]
Dy_4CoMg	Gd_4RhIn	$F\bar{4}3m$	1356.8(3)	a	a	2.4975	[39]
$Dy_{3.27}CoMg_{1.73}$	Gd_4RhIn	$F\bar{4}3m$	1344.8(2)	a	a	2.4321	[39]
$Dy_4Co_2Mg_3$	$Nd_4Co_2Mg_3$	$P2/m$	748.3(4)	371.07(9)	816.8(3) $\beta = 109.57(3)^\circ$	0.2137	[40]
Dy_2Ni_2Mg	Mo_2FeB_2	$P4/mbm$	739.0(1)	a	369.9(1)	0.2020	[26]
$DyCu_9Mg_2$	$TbCu_9Mg_2$	$P6_3/mmc$	500.04(3)	a	1620.84(11)	0.3510	[42]
Dy_2Cu_2Mg	Mo_2FeB_2	$P4/mbm$	759.93(9)	a	371.30(9)	0.2144	[29]
Dy_4RhMg	Gd_4RhIn	$F\bar{4}3m$	1366.9(1)	a	a	2.5537	[44]
Dy_2Pd_2Mg	Mo_2FeB_2	$P4/mbm$	765.2(2)	a	378.0(1)	0.2213	[35]
DyPdMg	ZrNiAl	$P\bar{6}2m$	742.5(1)	a	402.5(1)	0.1922	[41]
DyAgMg	ZrNiAl	$P\bar{6}2m$	764.5(2)	a	413.0(2)	0.2090	[41]
DyAuMg	ZrNiAl	$P\bar{6}2m$	752.2(2)	a	408.89(9)	0.2004	[28]
Ho_4CoMg	Gd_4RhIn	$F\bar{4}3m$	1348.6(2)	a	a	2.4526	[39]
Ho_2Ni_2Mg	Mo_2FeB_2	$P4/mbm$	737.8(2)	a	367.9(2)	0.2003	[26]
$HoCu_9Mg_2$	$TbCu_9Mg_2$	$P6_3/mmc$	498.89(8)	a	1621.49(15)	0.3495	[42]
Ho_2Cu_2Mg	Mo_2FeB_2	$P4/mbm$	758.67(5)	a	369.87(4)	0.2129	[29]
Ho_4RhMg	Gd_4RhIn	$F\bar{4}3m$	1362.3(1)	a	a	2.5283	[44]
$Ho_{3.52}RhMg_{1.48}$[a]	Gd_4RhIn	$F\bar{4}3m$	1355.7(2)	a	a	2.4917	[44]
Ho_2Pd_2Mg	Mo_2FeB_2	$P4/mbm$	764.57(7)	a	375.61(6)	0.2196	[35]
HoPdMg	ZrNiAl	$P\bar{6}2m$	742.2(1)	a	401.57(7)	0.1916	[35]
HoAgMg	ZrNiAl	$P\bar{6}2m$	763.32(8)	a	411.62(4)	0.2077	[30]
HoAuMg	ZrNiAl	$P\bar{6}2m$	750.9(2)	a	407.7(1)	0.1991	[28]
$Er_{3.72}CoMg_{1.28}$	Gd_4RhIn	$F\bar{4}3m$	1343.3(2)	a	a	2.4240	[39]
Er_2Ni_2Mg	Mo_2FeB_2	$P4/mbm$	734.07(4)	a	366.82(6)	0.1977	[26]
Er_2Cu_2Mg	Mo_2FeB_2	$P4/mbm$	756.18(3)	a	367.93(3)	0.2104	[29]
Er_4RhMg	Gd_4RhIn	$F\bar{4}3m$	1358.2(1)	a	a	2.5054	[44]
$Er_{3.94}RhMg_{1.06}$[a]	Gd_4RhIn	$F\bar{4}3m$	1355.4(2)	a	a	2.4900	[44]
ErPdMg	ZrNiAl	$P\bar{6}2m$	737.3(1)	a	401.8(1)	0.1892	[41]
ErAgMg	ZrNiAl	$P\bar{6}2m$	762.6(1)	a	407.4(1)	0.2052	[41]

Table 1 (*continued*)

Compound	Type	SG	*a* (pm)	*b* (pm)	*c* (pm)	*V* (nm^3)	Ref.
ErAuMg	ZrNiAl	$P\bar{6}2m$	747.4(1)	*a*	406.76(5)	0.1968	[28]
Tm_4CoMg	Gd_4RhIn	$F\bar{4}3m$	1337.6(3)	*a*	*a*	2.3930	[39]
Tm_2Ni_2Mg	Mo_2FeB_2	*P*4/*mbm*	734.39(8)	*a*	364.67(8)	0.1967	[26]
Tm_2Cu_2Mg	Mo_2FeB_2	*P*4/*mbm*	754.1(1)	*a*	365.3(4)	0.2077	[29]
Tm_4RhMg	Gd_4RhIn	$F\bar{4}3m$	1350.8(1)	*a*	*a*	2.4648	[44]
TmPdMg	ZrNiAl	$P\bar{6}2m$	735.9(2)	*a*	400.99(7)	0.1881	[35]
TmAgMg	ZrNiAl	$P\bar{6}2m$	759.9(2)	*a*	408.2(1)	0.2041	[30]
TmAuMg	ZrNiAl	$P\bar{6}2m$	746.4(1)	*a*	405.24(6)	0.1955	[28]
$YbCu_9Mg_2$	$TbCu_9Mg_2$	$P6_3/mmc$	501.91(3)	*a*	1618.02(13)	0.3530	[42]
$YbCu_4Mg$	$MgCu_4Sn$	$F\bar{4}3m$	719.4	*a*	*a*	0.3723	[58]
YbPdMg	TiNiSi	*Pnma*	729.4(2)	424.3(2)	850.5(3)	0.2632	[35]
YbPdMg	TiNiSi	*Pnma*	729.7(1)	425.4(1)	851.9(2)	0.2644	[43]
YbPdMg[a]	TiNiSi	*Pnma*	729.4(1)	425.2(1)	851.5(1)	0.2641	[43]
YbAgMg	TiNiSi	*Pnma*	753.66(7)	446.49(7)	887.2(1)	0.2986	[30]
YbAgMg	TiNiSi	*Pnma*	752.8(2)	445.9(1)	886.1(2)	0.2974	[43]
YbAgMg[a]	TiNiSi	*Pnma*	753.4(1)	446.3(1)	886.7(1)	0.2982	[43]
YbAuMg	TiNiSi	*Pnma*	738.4(1)	436.2(1)	864.6(2)	0.2785	[28]
$LuCu_4Mg$	$MgCu_4Sn$	$F\bar{4}3m$	712.9	*a*	*a*	0.3623	[58]
Lu_2Cu_2Mg	Mo_2FeB_2	*P*4/*mbm*	749.6(4)	*a*	359.9(4)	0.2022	[29]
Lu_4RhMg	Gd_4RhIn	$F\bar{4}3m$	1348.1(1)	*a*	*a*	2.4498	[44]

[a]Lattice parameters from single crystal data.

Table 2
Positional parameters of one representative for each structure type of the $RE_xT_yMg_z$ intermetallic compounds

Atom	Wyckoff site	x	y	z
$Nd_4Co_2Mg_3$ [38] (own type)				
Nd1	2*n*	0.60448	1/2	0.81696
Nd2	2*n*	0.09559	1/2	0.72365
Co	2*m*	0.6494	0	0.1056
Mg1	2*m*	0.2931	0	0.5007
Mg2	1*a*	0	0	0
PrAuMg [28] (ZrNiAl type)				
Pr	3*f*	0.58540	0	0
Au1	2*d*	1/3	2/3	1/2
Au2	1*a*	0	0	0
Mg	3*g*	0.2418	0	1/2
EuAuMg [28] (TiNiSi type)				
Eu	4*c*	0.03262	1/4	0.67659
Au	4*c*	0.27257	1/4	0.37621
Mg	4*c*	0.1393	1/4	0.0612
LaRhMg [32] (LaNiAl type)				
La1	4*c*	0.0438	1/4	0.28189
La2	4*c*	0.1623	1/4	0.06175
Rh1	4*c*	0.2447	1/4	0.43753
Rh2	4*c*	0.2535	1/4	0.6868
Mg1	4*c*	0.9971	1/4	0.5625
Mg2	4*c*	0.1329	1/4	0.8513
Ce_2Cu_2Mg [27] (Mo_2FeB_2 type)				
Ce	4*h*	0.17312	x + 1/2	1/2
Cu	4*g*	0.3798	x + 1/2	0
Mg	2*a*	0	0	0
$LaNiMg_2$ [45] ($MgCuAl_2$ type)				
La	4*c*	0	0.44029	1/4
Ni	4*c*	0	0.72661	1/4
Mg	8*f*	0	0.1543	0.0552
$PrNi_4Mg$ [22] ($MgCu_4Sn$ type)				
Pr	4*a*	0	0	0
Ni	16*e*	0.625	*x*	*x*
Mg	4*c*	1/4	1/4	1/4
Sm_4RhMg [44] (Gd_4RhIn type)				
Sm1	24*g*	0.56400	1/4	1/4
Sm2	24*f*	0.18798	0	0
Sm3	16*e*	0.34644	*x*	*x*
Rh	16*e*	0.14164	*x*	*x*
Mg	16*e*	0.5793	*x*	*x*
$TbCu_9Mg_2$ [42] (ordered $CeNi_3$ type)				
Tb	2*d*	1/3	2/3	3/4
Cu1	2*a*	0	0	0
Cu2	2*b*	0	0	1/4
Cu3	2*c*	1/3	2/3	1/4
Cu4	12*k*	0.1688	2*x*	0.1234
Mg	4*f*	1/3	2/3	0.5292
$LaNi_9Mg_2$ [21] ($PuNi_3$ type)				
La	3*a*	0	0	0
Ni1	3*b*	0	0	1/2
Ni2	6*c*	0	0	0.333
Ni3	18*h*	0.5015	−*x*	0.0857
Mg	6*c*	0	0	0.146
$CeCu_2Mg$ [46] ($ZrPt_2Al$ type)				
Ce	2*c*	1/3	2/3	1/4
Cu	4*f*	1/3	2/3	0.588
Mg	2*a*	0	0	0

Single crystal data of $CePd_{1.03}Mg_{0.97}$ [33], $CeRh_{1.262}Mg_{0.738}$ [32], $CeAg_{1.034}Mg_{0.966}$, and $NdAg_{1.035}Mg_{0.965}$ [30] revealed homogeneity ranges. Similar to the RE_2T_2Mg compounds discussed above, always the magnesium sites show mixing with the transition metal. Especially for $CeRh_{1.262}Mg_{0.738}$ the homogeneity range is pronounced and the largely differing Ce 4*f*–Rh 5*d* hybridization will strongly influence the magnetic properties. These investigations are currently in progress.

The *RET*Mg compounds with europium and ytterbium as rare earth component contain the rare earth atoms in a stable divalent oxidation state (see Section 4) and they crystallize with the orthorhombic TiNiSi type, space group *Pnma*. A view of the EuAuMg structure is presented in Fig. 3. Each gold atom has a strongly distorted tetrahedral magnesium coordination and vice versa. These $AuMg_{4/4}$ tetrahedra share all common corners, leading to a three-dimensional network in which the europium atoms fill larger cages. This structure type derives from the well known AlB_2 type via an ordering of the gold and magnesium atoms on the boron network and a strong puckering, leading to the substantial orthorhombic distortion [73]. Further details on TiNiSi type intermetallic compounds can be found in [70,74–77].

Similar to the ZrNiAl type equiatomic compounds, also $NdRh_{1.114}Mg_{0.886}$ [32], $EuAg_{1.032}Mg_{0.968}$, and $YbAg_{1.053}Mg_{0.947}$ [30] with the orthorhombic TiNiSi type structure show homogeneity ranges. Again, the rhodium-based compound shows the highest degree of Mg/Rh mixing.

The electronic structures of *RE*AuMg and *RE*AgMg (*RE* = Eu, Gd, Yb) have been determined experimentally through X-ray photoelectron spectroscopy [78]. The spectra clearly confirm the divalent character of europium and ytterbium and the trivalent character of gadolinium. The states at the Fermi level are dominated by a mix of Mg *s*, Au/Ag *s*/*p*, and *RE spd* bands. The photoelectron spectra reveal extremely narrow bandwidths for the Au and Ag *d* states, in good agreement with theoretical band structure calculations.

A peculiar structural arrangement has been observed for LaNiAl type [79] LaRhMg [32], space group *Pnma*. As is evident from the projection of the structure (Fig. 4), also the rhodium atoms in LaRhMg have trigonal prismatic coordination. The structure contains two crystallographically independent rhodium sites. The Rh1 atoms are located in trigonal prisms formed by four magnesium and two lanthanum atoms, while all Rh2 atoms have trigonal prismatic lanthanum coordination. The latter motif is also observed in the ZrNiAl type structure of PrAuMg (Fig. 2). It is interesting to note that the LaNiAl structure type has so far only been observed for ZrPdGa [80] and LaRhMg reported herein.

Finally, we should note that it is also possible to substitute the transition metal component in the RE_2T_2Mg and *RET*Mg compounds by a main group element (*M* = gallium, indium, thallium, silicon, or germanium), leading to compounds RE_2M_2Mg and *REM*Mg [81–88]

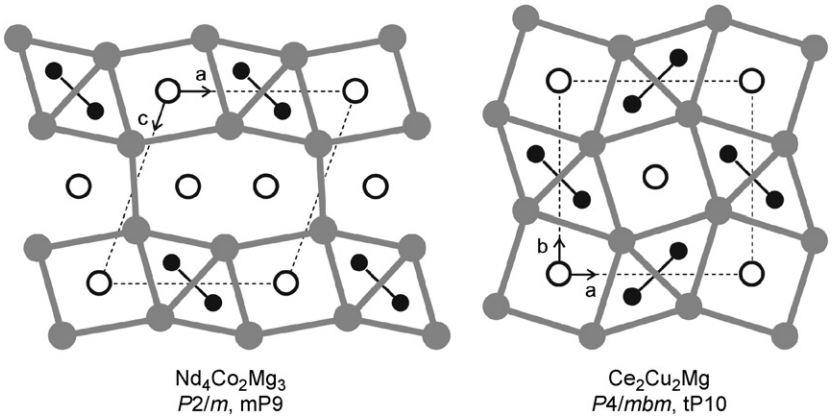

Fig. 1. Projections of the $Nd_4Co_2Mg_3$ and Ce_2Cu_2Mg structures along the short unit cell axis. Rare earth, transition metal and magnesium atoms are drawn as medium gray, black filled, and open circles, respectively. The distorted AlB_2 and CsCl related slabs and the transition metal dumb-bells are emphasized. All atoms lie on different mirror planes perpendicular to the projection directions.

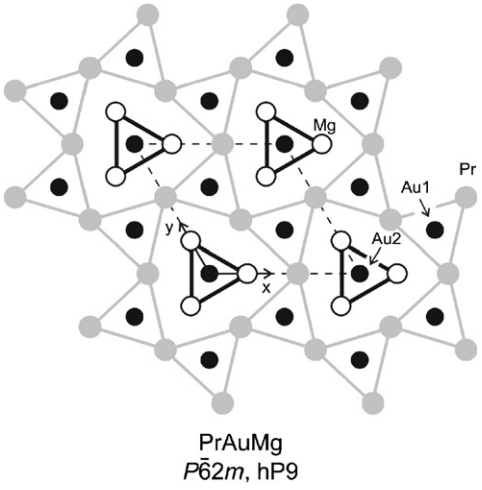

Fig. 2. Projection of the PrAuMg structure along the short unit cell axes. Praseodymium, gold, and magnesium atoms are drawn as medium gray, black filled, and open circles, respectively. The trigonal prismatic units are emphasized. All atoms lie on mirror planes at $z = 0$ (thin lines) and $z = 1/2$ (thick lines).

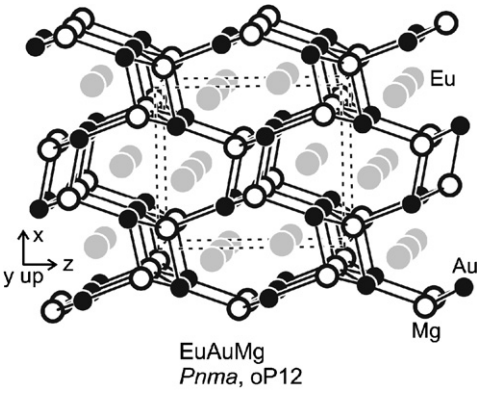

Fig. 3. View of the EuAuMg structure approximately along the *y*-axis. Europium, gold, and magnesium atoms are drawn as medium gray, black filled, and open circles, respectively. The three-dimensional [AuMg] network of distorted $AuMg_{4/4}$ tetrahedra is emphasized.

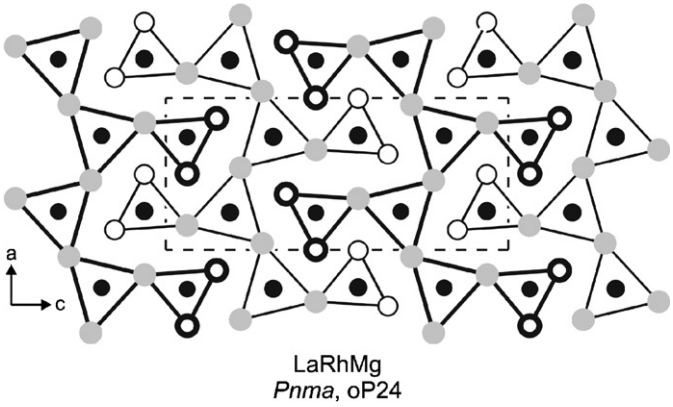

Fig. 4. Projection of the LaRhMg structure onto the *xz* plane. Lanthanum, rhodium, and magnesium atoms are drawn as medium gray, black filled, and open circles, respectively. All atoms lie on mirror planes at $y = 1/4$ (thin lines) and $y = 3/4$ (thick lines). The trigonal prismatic units are emphasized.

with similar structures. These substitutions have drastic effects on the magnetic properties.

3.3. The structure type $MgCuAl_2$

So far only one magnesium compound, $LaNiMg_2$ [45,53], crystallizes with the orthorhombic $MgCuAl_2$ type [89], space group *Cmcm*. First data on the crystal structure and hydrogenation behavior of $LaNiMg_2$ were reported by Kost et al. [53] and Karonik et al. [90,91]. The structure can be considered as a transition metal filled variant of the $CaIn_2$ type [92]. The magnesium atoms build up a tetrahedral network (Fig. 5) which is an orthorhombically distorted version of the hexagonal diamond structure, lonsdaleite. Within this network the Mg–Mg distances range from 303 to 331 pm, close to the average Mg–Mg distance of 320 pm in *hcp* magnesium [63]. Geometrically, these structures derive from the Re_3B type and the structural chemistry of these phases has been discussed in detail in [93]. Chemical bonding in $LaNiMg_2$ has been

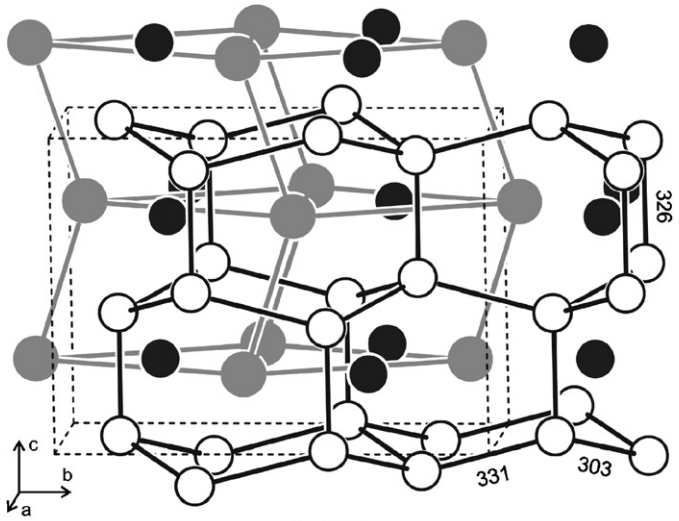

Fig. 5. Cutout of the $LaNiMg_2$ structure. Medium gray, black filled, and open circles represent lanthanum, nickel and magnesium atoms, respectively. Selected bond lengths within the magnesium substructure are given in pm.

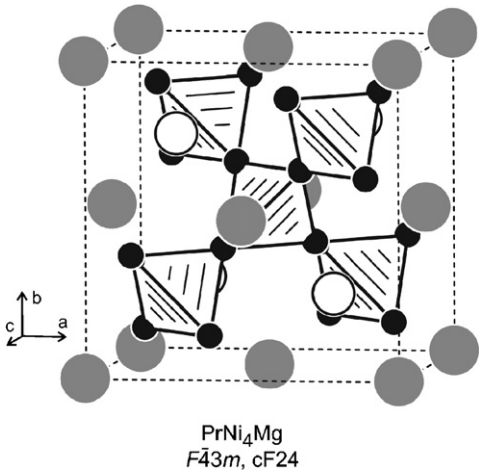

Fig. 6. The crystal structure of $PrNi_4Mg$. The praseodymium, nickel, and magnesium atoms are drawn as medium gray, filled, and open circles, respectively. The three-dimensional network of corner-sharing $Ni_{4/2}$ tetrahedra is emphasized.

analyzed on the basis of TB-LMTO-ASA electronic structure calculations in comparison with isotypic $LaNiCd_2$ and $LaPdIn_2$ [94]. The strongest bonding interactions in these three $LaTX_2$ compounds occur for the T–X contacts. An optimal bonding situation is observed for the Mg–Mg interactions in $LaNiMg_2$ and the Cd–Cd interactions in $LaNiCd_2$, where bonding states are almost completely filled. In contrast, the two extra electrons in $LaPdIn_2$ must occupy slightly antibonding states, which results in weaker In–In bonds.

3.4. The structure types $MgCu_4Sn$ and Gd_4RhIn

Many transition metal rich RET_4Mg magnesium compounds (Table 1) crystallize with an ordered version of the cubic Laves phase $MgCu_2$. They adopt the $MgCu_4Sn \equiv (Mg_{0.5}Sn_{0.5})Cu_2$ type [95,96]. This ordering (every other magnesium position is occupied by a rare earth atom) results in a *translationengleiche* symmetry reduction from space group $Fd\bar{3}m$ to $F\bar{4}3m$. The $PrNi_4Mg$ structure is presented as an example in Fig. 6. The nickel atoms build up a three-dimensional network of slightly distorted corner-sharing $Ni_{4/2}$ tetrahedra. The praseodymium and magnesium atoms fill larger cages of coordination number 16 (Frank–Kasper polyhedra [97,98]) within this network. The small distortion of the nickel tetrahedra is due to the difference in size between praseodymium and magnesium [10]. For a more detailed discussion on the crystal chemistry and chemical bonding in such Laves phases we refer to review articles [99–102, and references therein].

The RE_4TMg compounds (Table 1) represent the structure with the highest rare earth metal content. They crystallize with the cubic Gd_4RhIn [103,104] type, space

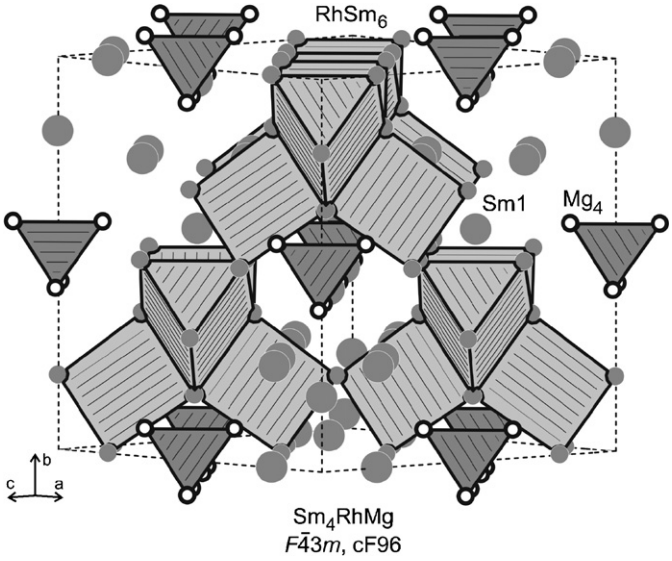

Fig. 7. View of the Sm_4RhMg crystal structure approximately along the [101] direction. Samarium, rhodium, and magnesium atoms are drawn as medium gray, filled (hidden in the trigonal prisms), and open circles, respectively. The three-dimensional network of corner-sharing $RhSm_6$ trigonal prisms and the Mg_4 tetrahedra are emphasized. The Sm1 atoms do not participate in the network of condensed trigonal prisms.

group $F\bar{4}3m$. As an example we present the Sm_4RhMg structure [44] in Fig. 7. The structure contains three crystallographically independent samarium sites. Together, the Sm2, Sm3, and Rh atoms build up a rigid three-dimensional network of corner-sharing trigonal prisms. The Rh–Sm distances of 286 pm are the shortest interatomic distances within the Sm_4RhMg structure and we can safely assume strong Rh–Sm bonding. This is in agreement with recent electronic structure calculations on isotypic La_4CoMg [39]. The voids left by the network of the $RhSm_6$ trigonal prisms is filled by a face-centered arrangement of

Mg_4 tetrahedra at Mg–Mg distances of 312 pm, even slightly smaller than in *hcp* magnesium (320 pm) [63]. Also the CN 14 polyhedra (10Sm + 2Rh + 2Mg) around Sm1 are located in the voids of the network. It is interesting to note, that the Gd_4RhIn type compounds have empty octahedral voids formed by the rare earth elements that can be filled by hydrogen.

The *RE*1 positions that do not belong to the trigonal prismatic network show *RE*1/Mg mixing in several of the RE_4TMg compounds. The compositions of several single crystals have been refined from diffractometer data: $Sm_{3.92}Co_{0.93}Mg_{1.08}$, $Gd_{3.92}CoMg_{1.08}$, $Tb_{3.77}CoMg_{1.23}$, $Dy_{3.27}CoMg_{1.73}$, and $Er_{3.72}CoMg_{1.28}$ for the cobalt [39], and $Ho_{3.52}RhMg_{1.48}$, and $Er_{3.94}RhMg_{1.06}$ for the rhodium [44] based series.

3.5. The structure types $PuNi_3$ and $CeNi_3$

The series of REMg$_2$Ni$_9$ (RE = Y, La–Nd, Sm, Gd) [21,49,105] and REMg$_2$Cu$_9$ (RE = Y, La–Nd, Sm–Ho, Yb) [42], and a substitution variant $(Y_{0.5}Ca_{0.5})$(MgCa)Ni_9 have intensively been investigated with respect to their hydrogenation capacity. The nickel-based series is isotypic with the $PuNi_3$ type [106], space group $R\bar{3}m$, while the copper compounds adopt the $CeNi_3$ type [107], space group $P6_3/mmc$. In both series, 2/3 of the rare earth sites of the binaries are replaced in an ordered manner by magnesium. This fact is not astonishing, in view of the *RE*1/Mg substitution discussed for the Gd_4RhIn type materials (see Section 3.4).

Both structure types have relatively long *c*-axis, i.e. ≈23 Å for the REMg$_2$Ni$_9$ and ≈16 Å for the REMg$_2$Cu$_9$ compounds. They belong to a larger family of intermetallic compounds that can be considered as block stacking structures. As already emphasized in an overview by Parthé and Lemaire [108], the $CeNi_3$ and $PuNi_3$ structures are stacking variants of simple $MgZn_2$ and $CaCu_5$ related slabs. Consequently, all atoms in these structures have comparatively high coordination numbers and the coordination polyhedra resemble the well known Frank Kasper polyhedra [97,98]. A polyhedral presentation of both structure types is given in Fig. 8. Separate drawings of the different coordination polyhedra for $TbCu_9Mg_2$ can be found in Ref. [42].

Exemplary we briefly discuss the $TbCu_9Mg_2$ structure here. The highest coordination numbers (CN) occur for the terbium (CN 20) and magnesium (CN 16) atoms. The four crystallographically independent copper sites have all icosahedral, Frank–Kasper type coordination. The Cu–Cu distances within the complex three-dimensional $[Mg_2Cu_9]$ network range from 246 to 289 pm, close to the Cu–Cu distance of 256 pm in *fcc* copper [63]. For comparison, the Cu–Cu distances in Ce_2Cu_2Mg (268 pm) [27] and $CeCu_2Mg$ (280 pm) [46] fall in the same range. The Cu–Mg distances (287–299 pm) in $TbCu_9Mg_2$ [42] are slightly longer than in the $CeCu_2Mg$ structure (279 pm) [46]. Similar coordination behavior is observed in the nickel-based series.

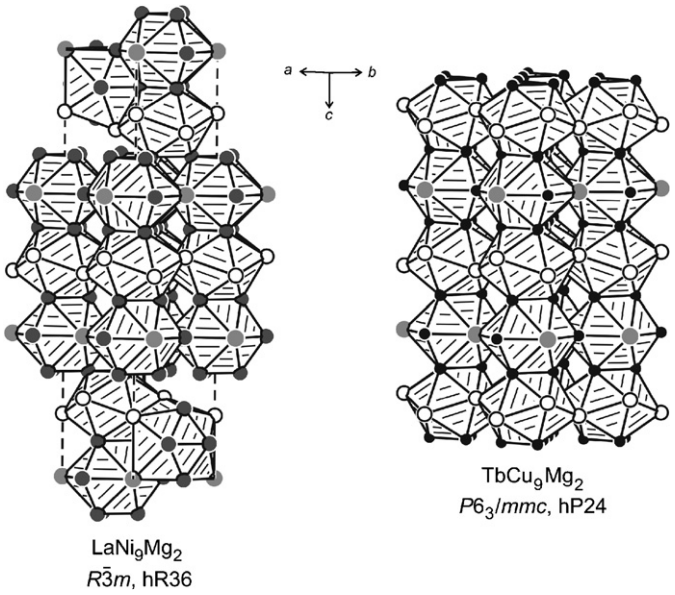

Fig. 8. The crystal structures of $LaNi_9Mg_2$ and $TbCu_9Mg_2$. Rare earth metal, transition metal, and magnesium atoms are drawn as medium gray, filled, and open circles, respectively. The Frank–Kasper related polyhedra are emphasized. For details see text.

3.6. The structure type $ZrPt_2Al$

The magnesium compounds $LaCu_2Mg$ and $CeCu_2Mg$ [46,56] crystallize with the hexagonal $ZrPt_2Al$ [109] type structure, space group $P6_3/mmc$, which has also been observed for a series of stannides [110] and indides [111]. This structure type can be considered as a substitution variant of the Ni_2In type, where the nickel sites within the Ni_3In_3 hexagonal honeycomb networks are substituted by a dumb-bell. The Cu_2 pairs (280 pm Cu–Cu) and the cerium atoms in these two compounds have trigonal prismatic magnesium coordination (Fig. 9). Together the copper and magnesium atoms (279 pm Cu–Mg) build up a three-dimensional $[Cu_2Mg]$ network in which the cerium atoms fill larger cages. The Cu–Cu distances in $CeCu_2Mg$ are close to the distances in Ce_2Cu_2Mg (268 pm), while the Cu–Mg distances at 314 pm in Ce_2Cu_2Mg are much longer [27]. Finally we need to mention that the structures of $ZrPt_2Al$ [109], the stannides [110] and indides [111], as well as $CeCu_2Mg$ [46] have only been studied on the basis of powder X-ray diffraction data. In can therefore not be excluded, that some Ce/Mg mixing might occur in $CeCu_2Mg$, as already stated for $GdPt_2Sn$ and $ErPt_2Sn$ [110].

4. Physical properties

4.1. Magnetic susceptibility

Many of the $RE_xT_yMg_z$ compounds have been studied with respect to their magnetic properties (Table 3). The lanthanum and cerium based series LaTMg and CeTMg (T = Pd, Pt, Au) [33] have been investigated in detail.

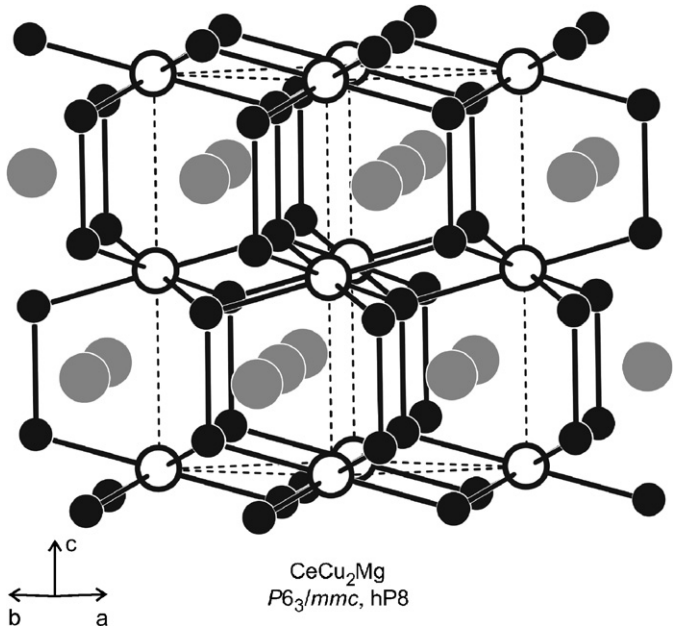

Fig. 9. The crystal structure of $CeCu_2Mg$. Cerium, copper, and magnesium atoms are drawn as medium gray, filled, and open circles, respectively. The three-dimensional $[Cu_2Mg]$ network and the trigonal prismatic units are emphasized.

All three lanthanum compounds show Pauli paramagnetism down to 0.3 K. Cerium is in a stable trivalent oxidation state in the Ce*T*Mg (T = Pd, Pt, Au) compounds. Magnetic ordering is detected at 2.1(2), 3.6(2), and 2.0(2) K, for CePdMg, CePtMg, and CeAuMg, respectively.

The magnetic properties of CePdMg, Ce_2Ni_2Mg, and $CeNi_4Mg$ have been studied by Geibel et al. [47]. In contrast to the investigation by Gibson et al. [33], no magnetic ordering has been reported for CePdMg. Ce_2Ni_2Mg, and $CeNi_4Mg$ are intermediate-valent compounds. The characteristic temperature for the cerium 4*f* electrons $E_f/k_B \approx T_m \approx 250$ K was deduced from the maximum in the $\chi(T)$ curve. For $CeNi_4Mg$ E_f/k_B is probably larger than 300 K.

Very interesting magnetization behavior is observed for Nd_2Cu_2Mg [115] and Pr_2Pd_2Mg [35]. Both compounds show a pronounced square loop behavior, Nd_2Cu_2Mg [115] in the ferromagnetically ordered state and Pr_2Pd_2Mg [35] in the metamagnetic regime. Nd_2Cu_2Mg [115] shows a relatively high remanent magnetization of 1.55 μ_B/Nd atom and a coercive field of 0.31 T.

The gadolinium compounds Gd*T*Mg (T = Pd, Ag, Pt) show relatively high Curie temperatures of 95.7(1), 39.3(1), and 97.6(1) K, respectively [34]. These materials reveal spin reorientations at 93.2(1) (GdPdMg), 27.6(2) (GdAgMg), and 65.3(1) and 89.2(1) K (GdPtMg). The three compounds are typical soft ferromagnets. The magnetization curves for GdPdMg and GdPtMg show full saturation already at 2 T, while GdAgMg reveals a much smaller (4.82 μ_B/Gd atom) saturation magnetization at 4.23 K and 5.5 T.

Table 3
Magnetic properties of various intermetallic $RE_xT_yMg_z$ compounds

Compound	Magnetism	μ_{exp}/μ_B	T_N, T_C/K	Θ/K	Ref.
Y_2Cu_2Mg	PP	—	—	—	[115]
La_2Cu_2Mg	PP	—	—	—	[115]
LaPdMg	PP	—	—	—	[33]
LaAgMg	PP	—	—	—	[113]
LaPtMg	PP	—	—	—	[33]
LaAuMg	PP	—	—	—	[33]
Ce_2Ni_2Mg	IV	—	—	—	[47]
$CeNi_4Mg$	IV	—	—	—	[47]
$CeCu_2Mg$	P	2.46	—	−20	[46]
CePdMg	F	2.6(1)	2.1(2)	−36(1)	[33]
CeAgMg	P	2.52(2)	—	−13(1)	[113]
CePdMg	P	2.6	—	−33	[47]
CePtMg	F	2.5(1)	3.6(2)	−35(1)	[33]
CeAuMg	AF	2.6(1)	2.0(2)	−57(1)	[33]
Pr_2Cu_2Mg	F	3.47(2)	43.0(5)	−5(1)	[115]
Pr_2Pd_2Mg	MM	3.86(5)	15(1)	23(1)	[35]
PrPtMg	F	3.59(2)	8.0(5)	7.5(5)	[31]
Nd_2Cu_2Mg	F	3.67(2)	12.0(5)	6(1)	[115]
Sm_2Pd_2Mg	VVP/F	—	36(2)	—	[35]
SmPtMg	VVP/F	—	52(1)	—	[31]
EuAgMg	F	7.99(5)	22.0(3)	—	[113]
EuAuMg	F	7.80(5)	36.5(5)	—	[113]
Gd_2Ni_2Mg	AF	7.86	49.00(5)	49	[112]
GdPdMg	F	7.66	95.7(1)	91(1)	[34]
GdAgMg	F	8.05	39.3(1)	31.9(5)	[34]
GdPtMg	F	8.27	97.6(1)	90.9(5)	[34]
GdAuMg	AF	8.35	81.1(1); 19.0(1)	12.7	[36]
YbPdMg	PP	—	—	—	[35,43]
YbAgMg	PP	—	—	—	[43,113]
YbAuMg	PP	—	—	—	[114]

PP: Pauli paramagnet, P: paramagnet, AF: antiferromagnet, F: ferromagnet, MM: metamagnetism, IV: intermediate valence, VVP: van Vleck paramagnetism, T_N: Néel temperature, T_C: Curie temperature, μ_{exp}: experimental magnetic moment, Θ: paramagnetic Curie temperature (Weiss constant).

The complete solid solution $CeAuIn_{1-x}Mg_x$ has been studied with respect to the magnetic properties [37]. Both boundary phases CeAuIn and CeAuMg crystallize with the ZrNiAl type structure and single crystal data reveal that a Vegard type behavior occurs for the solid solution. The chemical substitution creates disorder and consequently destroys long-range magnetic ordering. The compounds within the solid solution show features of non-Fermi liquid behavior.

$YbCu_4Mg$ with cubic $MgCu_4Sn$ type structure has intensively been studied within the whole series of $YbCu_4X$ (X = Ag, Au, In, Cd, Tl, Mg) compounds [58,116–120]. $YbCu_4Mg$ is a Kondo compound with a Kondo temperature of ca. 860 K and a γ-value of 60 mJ/molK^2 [116]. Hall effect measurements reveal small, negative, only weakly temperature-dependent Hall coefficients [117]. Photoemission spectra [118] show that the Yb^{2+} $4f_{7/2}$ states of $YbCu_4Mg$ are observed as a broad structure near the Fermi level and the valence is close to divalent [120]. The magnetic susceptibility is only weakly temperature-dependent with a small positive value of ca. 0.004 emu/mol

[58,119]. It is interesting to note that single crystals of $YbCu_4Mg$ can be grown from a lead flux [58].

4.2. Specific heat data

So far only few of the rare earth–transition metal–magnesium compounds have been studied with respect to the temperature dependence of the specific heat. Complete measurements of the specific heat data are available for the series La*T*Mg and Ce*T*Mg (*T* = Pd, Pt, Au) [33]. These compounds show very small values for the electronic specific heat coefficients. In contrast, a huge γ-value of 1000 mJ/mol K^2 was observed for the Kondo compound $CeCu_2Mg$ [46], however, no long-range magnetic ordering was evident above 1.5 K.

4.3. Electrical resistivity

The rare earth–transition metal–magnesium compounds exhibit all metallic behavior in the temperature dependence of the electric resistivity, in agreement with the electronic structure investigations. Detailed resistivity data have been collected for Ce*T*Mg (*T* = Pd, Pt, Au) [33], *RE*AgMg (*RE* = La, Ce, Eu, Yb) and EuAuMg [121]. Since these magnesium intermetallics have been prepared in sealed tantalum containers, the product pieces were mechanically broken off the ampoules, resulting in small, irregularly shaped blocks. Thus, resistivity data have been measured either on small sintered pellets or on irregularity shaped pieces and only resistivity ratios $\rho(T)/\rho(300\,K)$ have been reported. The cerium compounds Ce*T*Mg (*T* = Pd, Ag, Pt, Au) [33,113], show negative curvature of $\rho(T)$ below ca. 100 K, which could arise from CEF level population which causes an additional temperature dependence of the spin disorder resistivity. EuAgMg and EuAuMg [113] show strong discontinuities in the temperature dependence of the resistivity at 20 and 36 K, that can be attributed to freezing of spin-disorder scattering below the Curie temperatures, in agreement with the magnetic data (Table 3).

Intermediate-valent and Kondo type materials show pronounced anomalies in the temperature dependence of the electrical resistivity. $CeCu_2Mg$ [46] reveals a maximum in the $\rho(T)$ curve, indicating Kondo lattice behavior. The Kondo temperature was estimated to be $T_K \approx |\Theta_P|/4 = 5$ K. A weak Kondo interaction occurs also in the resistivity behavior of CePdMg [47]. A pronounced curvature of the $\rho(T)$ curve was observed for intermediate-valent Ce_2Ni_2Mg, while $CeNi_4Mg$ shows almost linear behavior [47].

The compounds *RE*AgMg and *RE*AuMg (*RE* = La, Eu, Gd, Yb) have been investigated with respect to their magnetoresistance behavior [121]. All compounds show a metallic resistivity. The magnetically ordering ones (with *RE* = Eu and Gd) reveal an abrupt decrease of the resistivity below the Curie and Néel temperatures, because the scattering of charge carriers on magnetic excitations freezes out in the magnetically ordered state. For the ferromagnets a large negative magnetoresistance (most pronounced close to T_C) is observed with a decrease of ρ in the order of -5%/T, while the antiferromagnetic ones show a much smaller rate (-0.2%/T). Similar trend is observed for the magnetocaloric effect.

4.4. Mössbauer spectroscopy

So far, only EuAgMg, EuAuMg [113], GdAuMg [36] and Gd_2Ni_2Mg [112] have been characterized by Mössbauer spectroscopy. These data are especially important for the europium compounds for determination of the europium valence. The 78 K ^{151}Eu Mössbauer spectra of EuAgMg and EuAuMg [113] show isomer shift of $\delta = -9.00(4)$ and $-8.72(8)$ mm/s, respectively, indicative for a slightly lower electron density at the Eu nuclei in EuAuMg, a consequence of the higher electronegativity of gold with respect to silver. The magnetic ordering temperatures determined from the temperature dependence of the magnetic hyperfine fields (fits to a $J = 7/2$ Brillouin function) are in good agreement with the susceptibility data. At 4.2 K full magnetic hyperfine field splitting with hyperfine fields of 17.4(1) and 18.3(2) T are observed for EuAgMg and EuAuMg.

Magnetic ordering in GdAuMg was also detected via ^{155}Gd Mössbauer spectroscopy [36]. Due to the low *m*2*m* Gd site symmetry a quadrupole splitting parameter of $\Delta E_Q = 0.646(7)$ mm/s is detected. A small magnetic hyperfine field of 16.5(5) T was observed at 4.2 K, indicating that the antiferromagnetic interactions are still strong. The isomer shift of $\delta = 0.294(8)$ mm/s indicates relative high electron density at the Gd nuclei in GdAuMg as compared to isotypic GdAuIn with the more electronegative indium atoms. Similar value (0.272(3) mm/s) occurs for GdAgMg, while GdPdMg (0.192(7) mm/s) and GdPtMg (0.190(4) mm/s) show lower isomer shifts, clearly indicating the influence of the valence electron concentration [34]. The hyperfine fields at 4.2 K of 21.2(2) T (GdPdMg), 21.4(1) T (GdAgMg), and 18.8(2) T (GdPtMg) are slightly higher than for GdAuMg.

Gd_2Ni_2Mg [112] shows an isomer shift of $\delta = 0.12(1)$ mm/s at 57 K in the paramagnetic range. The observed quadrupole splitting parameter of $\Delta E_Q = 3.17(3)$ mm/s is a direct consequence of the *m*2*m* Gd site symmetry. At 4.2 K, in the magnetically ordered state, a magnetic hyperfine field of 14.6(2) T is detected at the gadolinium nuclei.

5. Hydrogenation behavior

In continuation to the research on Ni–MH batteries, the search for alternative hydrogen storage materials is an extremely active field. The extensive studies on Mg_2NiH_4 and related hydrides have been extended towards rare earth based intermetallic compounds in recent years [122–140]. The rare earth–transition metal–magnesium compounds are currently widely investigated with respect to their

hydrogen storage capacity. Since many $CaCu_5$ and Laves phase related materials have been studied intensively in recent years, also ternary materials with related structures have been synthesized (see Section 3.5). Structure stability maps for intermetallic AB_5 compounds with respect to hydrogen storage materials have been developed by Guénée and Yvon [141].

Especially the $MgCu_4Sn$ type materials like $RENi_4Mg$ (RE = Y, La, Ce, Pr, Nd) have intensively been studied [57,123,124,132,133]. These compounds reveal excellent discharge capacities in the order of 400 mAh/g and only a slight decrease of the discharge stability over a period of 50 cycles. Besides the influence of the different rare earth components, also the influence of Co/Ni substitution on the tetrahedral network was tested. Cobalt seems to enhance the hydrogenation properties [132]. The article size has a drastic influence on the discharge capacity [124,134] and mechanical alloying improves the kinetic properties. This can be explained by the defects introduced during the mechanical alloying process as well as the increased specific surface area. The solid solution $GdNi_{4-x}Al_xMg$, prepared by mechanical alloying, shows reversible hydrogen absorption and desorption at room temperature [142].

The hydrogenation behavior of the ordered Laves phases YNi_4Mg [59], $LaNi_4Mg$, and $NdNi_4Mg$ [15] has been studied in detail. For the yttrium compound a maximum hydrogen content H/M of ca. 0.6 was observed. $LaNi_4Mg$, and $NdNi_4Mg$ [15] reversibly uptake up to four hydrogen atoms per formula unit at 7–8 bar and 323 K. The structure of the hydride was determined from neutron diffraction data on a deuterated sample $NdNi_4MgH_{3.6}$. The striking structural motif in this hydride phase in a Ni_4D_4 unit. The Ni_4 tetrahedra are capped by three deuterium atoms on the edges, and by a fourth deuterium atom on the remaining triangular face.

Two highly interesting hydrogenation experiments start from the intermetallic phases La_2Ni_2Mg (Mo_2B_2Fe type) and $LaNiMg_2$ ($MgCuAl_2$ type), leading to the hydrides $La_2Ni_2MgH_8$ [143] and $LaNiMg_2H_7$ [45,53]. $La_2Ni_2MgH_8$ forms under 30 bar of hydrogen pressure at 373 K (lattice expansion $\Delta V/V = 20\%$) and $LaNiMg_2H_7$ at 473 K with 8 bar H_2 (lattice expansion $\Delta V/V = 19.1\%$). The $LaNiMg_2H_7$ structure contains $[NiH_4]^{4-}$ tetrahedral hydridometallate units that are conform with the 18-electron rule besides H^- anions leading to an ionic formula splitting $La^{3+}(2Mg^{2+})^{4+}[NiH_4]^{4-}(3\,H^-)^{3-}$. Thus, the intermetallic compound $LaNiMg_2$ had transformed to the non-metallic hydride $LaNiMg_2H_7$. In agreement with the ionic formula splitting the hydrogenation induces a metal–semiconductor transition as is evident from resistivity measurements on compact polycrystalline samples of $LaNiMg_2$ and $LaNiMg_2H_7$ [144].

The bonding situation in $La_2Ni_2MgH_8$ is somewhat more complex. This hydride contains a $[Ni_2H_7]^{7-}$ unit (two corner-sharing tetrahedra) and a cyclic $[Ni_4H_{12}]^{12-}$ hydridonickelate complex (four corner-sharing tetrahedra). Again, an ionic formula splitting is adequate: $4La_2Ni_2MgH_8 \equiv (8La^{3+})^{24+}(4Mg^{2+})^{8+}[Ni_4H_{12}]^{12-}[2Ni_2H_7^{7-}]^{14-}(6\,H^-)^{6-}$, in agreement with the 18-electron rule. Thus, in both hydrides the nickel atoms are essentially neutral with sp^3 hybridized valence orbitals. $La_2Ni_2MgH_8$ does not reversibly desorb hydrogen. Upon heating at 673 K over 24 h $La_2Ni_2MgH_8$ decomposes into LaH_3 and another phase.

In this context we should also mention the hydrides $Yb_4Fe_3Mg_4H_{22}$ [145] and $Yb_4Co_3Mg_4H_{19}$ [146] which contain disordered square-pyramidal $[CoH_5]^{4-}$ and octahedral $[FeH_6]^{4-}$ units, respectively, leading to the following ionic formula splittings: $(4Yb^{2+})^{8+}(4Mg^{2+})^{8+}[3FeH_6^{4-}]^{12-}(4\,H^-)^{4-}$ and $(4Yb^{2+})^{8+}(4Mg^{2+})^{8+}[3CoH_5^{4-}]^{12-}(4\,H^-)^{4-}$, where the hydridometallate anions contain divalent iron (d^6) and monovalent cobalt (d^8). In contrast to $La_2Ni_2MgH_8$ and $LaNiMg_2H_7$ discussed above, no ternary intermetallic compounds '$Yb_4Fe_3Mg_4$' and '$Yb_4Co_3Mg_4$' have been reported so far. In the La–Cu–Mg system a new hexagonal compound with approximate composition $LaCu_2Mg_2$ has been reported [51]. The crystal structure is not yet known, however, $LaCu_2Mg_2$ shows a hydrogen uptake up to 2.4 wt.−% and a reasonable desorption pressure.

Besides the Laves phase related materials, also the stacking variants of the $MgZn_2$ and $CaCu_5$ slabs have intensively been studied with respect to solid solutions [122,125,126–131,135–140]. These materials are all substitution variants of the $PuNi_3$, $CeNi_3$, Gd_2Co_7, or Ce_2Ni_7 types. Detailed electrochemical studies of the hydrides showed good cycle stability and comparatively high discharge capacities up to 400 mAh/g. Some compounds in the La–Ni–Mg system revealed even capacity retention of ca. 82% after 150 charge/discharge cycles [139]. Several samples are composites of different phases [135]. Depending on the peculiar system, Co/Ni substitution can have a positive or a negative influence on the discharge capacity [131,135,140]. This behavior was also studied via electrochemical impedance spectra [135]. Another substitution concerns the rare earth component. The RE_2MgNi_9 materials have also been tested with the cheaper misch metal on the rare earth site. As compared to La_2MgNi_9, the misch metal based alloy electrode shows improved dischargeability rates [130]. Doping with B, Cr, or Ti was also tested [137].

Hydrogenation studies revealed no hydrogen absorption for YMg_2Ni_9, while $(Y_{0.5}Ca_{0.5})(MgCa)Ni_9$ forms a hydride phase $(Y_{0.5}Ca_{0.5})(MgCa)Ni_9H_{13.2}$ at 3.3 MPa and 263 K [49]. $(Y_{0.5}Ca_{0.5})(MgCa)Ni_9H_{13.2}$ shows linearity in the van't Hoff plot for hydrogen desorption. Substitution in the YMg_2Ni_9 structure on the yttrium and the magnesium site by calcium clearly establishes that the hydrogenation behavior depends on geometric and electronic factors as well.

An interesting substitution occurs for the $NiMg_2$ phase [147–149]. Besides the solid solution $NiMg_{2-x}Sn_x$ [150], also $NiMg_{2-x}RE_x$ (up to $x = 0.3$ and RE = Y, La, Ce, Pr, Nd)

solid solutions have been reported [57]. These materials can easily be prepared by ball-milling and the hydrogenation properties improve with increasing rare earth content. For the various rare earth metals, the discharge capacity increased in the order Pr > Nd > Ce > La > Y.

The kinetics of the hydrogen absorption/desorption properties strongly depends on the sample preparation and the particle size [122,125–129]. Ball milling and melt spinning play an important role on the microstructure and surface morphology [122,128]. In the melt spun materials, the hydrogen transport along the nanograin boundaries appears to facilitate the desorption kinetics [127]. For the ball milling process, also the medium in the containers (argon, toluene, or tetrahydrofuran) influence the surface properties [128]. Hydrogen combustion synthesis [126,151] with and without magnetic field influence the microstructure and the phase composition and can drastically improve the absorption/desorption kinetics [129].

The annealing behavior of melt spun materials is interesting to mention [19,122,152–157]. To give an example, a melt spun amorphous $Mg_{65}Cu_{25}Nd_{10}$ alloy shows a first crystallization reaction at 180 °C, a second at 210–225 °C, and a third one at 320 °C (exothermic reaction) [122]. The resulting crystalline compounds are exclusively binary ones, i.e. $CuMg_2$, α-Mg, and $NdCu_5$, and such composites show good hydrogenation properties. No ternaries like Nd_2Cu_2Mg [29] are observed. It is interesting to note that the glass-forming magnesium-based alloys have good stability in aqueous electrolytes [122].

6. Conclusions

So far more than 170 $RE_xT_yMg_z$ compounds have been synthesized in the ternary systems *RE*–*T*–Mg. However, the phase diagrams have only scarcely been investigated. The intermetallic $RE_xT_yMg_z$ compounds show interesting crystal chemistry and fascinating bonding peculiarities when compared with crystal chemically related indides and stannides. These materials have excellent perspectives for hydrogen storage materials and are worthwhile to investigate in future.

Acknowledgments

This work was financially supported by the Deutsche Forschungsgemeinschaft. B.C. and R.P. are indebted to EGIDE and DAAD for research grants within the PROCOPE programs (11457RD and D/0502176). Finally, B.C. thanks the European Science Foundation (ECOM_COST action P16) for financial support.

References

[1] K.U. Kainer (Ed.), Magnesium, Proceedings of the 6th International Conference on Magnesium Alloys and their Applications, Wiley, VCH, Weinheim, 2004.
[2] R. Pöttgen, R.-D. Hoffmann, Metall 58 (2004) 557.
[3] N. Hort, Yu. Huang, K.U. Kainer, Adv. Eng. Mater. 8 (2006) 235.
[4] J.J. Reilly, R.H. Wiswall Jr., Inorg. Chem. 6 (1967) 2220.
[5] J.J. Reilly, R.H. Wiswall Jr., Inorg. Chem. 7 (1968) 2254.
[6] H. Nagai, H. Tomizawa, T. Ogasawara, K. Shoji, J. Less-Common Met. 157 (1990) 15.
[7] Ye. Zhou, L.C. Erickson, B. Hjörvasson, J. Alloys Compd. 209 (1994) 117.
[8] S.S. Sai Raman, O.N. Srivastata, Int. J. Hydrogen Energy 21 (1996) 207.
[9] R. Pöttgen, D. Johrendt, Chem. Mater. 12 (2000) 875.
[10] J. Emsley, The Elements, Oxford University Press, Oxford, 1999.
[11] J.D. Corbett, Inorg. Synth. 22 (1983) 15.
[12] R. Pöttgen, T. Gulden, A. Simon, GIT Labor-Fachzeitschrift 43 (1999) 133.
[13] D. Kußmann, R.-D. Hoffmann, R. Pöttgen, Z. Anorg. Allg. Chem. 624 (1998) 1727.
[14] R. Pöttgen, A. Lang, R.-D. Hoffmann, B. Künnen, G. Kotzyba, R. Müllmann, B.D. Mosel, C. Rosenhahn, Z. Kristallogr. 214 (1999) 143.
[15] L. Guénée, V. Favre-Nicolin, K. Yvon, J. Alloys Compd. 348 (2003) 129.
[16] L. Zaluski, A. Zaluska, J.O. Ström-Olsen, J. Alloys Compd. 253–254 (1997) 70.
[17] S. Orimo, H. Fujii, K. Ikeda, Acta Mater. 45 (1997) 331.
[18] M. Zhu, C.H. Peng, L.Z. Ouyang, Y.Q. Tong, J. Alloys Compd. 426 (2006) 316.
[19] T. Spassov, V. Rangelova, N. Neykov, J. Alloys Compd. 334 (2002) 219.
[20] L.J. Huang, G.Y. Liang, Z.B. Sun, J. Alloys Compd. 421 (2006) 279.
[21] K. Kadir, T. Sakai, I. Uehara, J. Alloys Compd. 257 (1997) 115.
[22] K. Kadir, D. Noréus, I. Yamashita, J. Alloys Compd. 345 (2002) 140.
[23] Q. Yao, H. Zhou, Zh. Wang, J. Alloys Compd. 421 (2006) 117.
[24] H. Zhou, Y. Wang, Q. Yao, J. Alloys Compd. 407 (2006) 129.
[25] Z. Huaiying, X. Xin, Ch. Gang, W. Zhongmin, Zh. Songli, J. Alloys Compd. 386 (2005) 144.
[26] R.-D. Hoffmann, A. Fugmann, U. Ch. Rodewald, R. Pöttgen, Z. Anorg. Allg. Chem. 626 (2000) 1733.
[27] R. Pöttgen, A. Fugmann, R.-D. Hoffmann, U. Ch. Rodewald, D. Niepmann, Z. Naturforsch. 55b (2000) 155.
[28] R. Pöttgen, R.-D. Hoffmann, J. Renger, U. Ch. Rodewald, M.H. Möller, Z. Anorg. Allg. Chem. 626 (2000) 2257.
[29] R. Mishra, R.-D. Hoffmann, R. Pöttgen, Z. Naturforsch. 56b (2001) 239.
[30] Th. Fickenscher, R. Pöttgen, J. Solid State Chem. 161 (2001) 67.
[31] R. Kraft, G. Kotzyba, R.-D. Hoffmann, R. Pöttgen, Z. Naturforsch. 57b (2002) 488.
[32] Th. Fickenscher, R.-D. Hoffmann, R. Kraft, R. Pöttgen, Z. Anorg. Allg. Chem. 628 (2002) 667.
[33] B.J. Gibson, A. Das, R.K. Kremer, R.-D. Hoffmann, R. Pöttgen, J. Phys. C 14 (2002) 5173.
[34] K. Łątka, T. Tomkowicz, R. Kmieć, A.W. Pacyna, R. Mishra, R.-D. Hoffmann, T. Fickenscher, R. Pöttgen, H. Piotrowski, J. Solid State Chem. 168 (2002) 331.
[35] R. Kraft, Th. Fickenscher, G. Kotzyba, R.-D. Hoffmann, R. Pöttgen, Intermetallics 11 (2003) 111.
[36] K. Łątka, R. Kmieć, A.W. Pacyna, Th. Fickenscher, R.-D. Hoffmann, R. Pöttgen, Solid State Sci. 6 (2004) 301.
[37] S. Rayaprol, B. Heying, R. Pöttgen, Z. Naturforsch. 61b (2006) 495.
[38] S. Tuncel, R.-D. Hoffmann, B. Heying, B. Chevalier, R. Pöttgen, Z. Anorg. Allg. Chem. 632 (2006) 2017.
[39] S. Tuncel, R.-D. Hoffmann, B. Chevalier, S.F. Matar, R. Pöttgen, Z. Anorg. Allg. Chem. 633 (2007) 151.
[40] S. Tuncel, U. Ch. Rodewald, S.F. Matar, B. Chevalier, R. Pöttgen, Z. Naturforsch. 62b (2007) 162.
[41] A. Iandelli, J. Alloys Compd. 203 (1994) 137.

[42] P. Solokha, V. Pavlyuk, A. Saccone, S. De Negri, W. Prochwicz, B. Marciniak, E. Różycka-Sokołowska, J. Solid State Chem. 179 (2006) 3073.
[43] M.L. Fornasini, F. Merlo, M. Napoletano, M. Pani, J. Phase Equilibria 23 (2002) 57.
[44] S. Tuncel, U. Ch. Rodewald, B. Chevalier, R. Pöttgen, Z. Naturforsch. 62b (2007), in press.
[45] G. Renaudin, L. Guénée, K. Yvon, J. Alloys Compd. 350 (2003) 145.
[46] M. Giovannini, E. Bauer, G. Hilscher, R. Lackner, H. Michor, A. Saccone, Physica B 378–380 (2006) 831.
[47] C. Geibel, U. Klinger, M. Weiden, B. Buschinger, F. Steglich, Physica B 237–238 (1997) 202.
[48] B.J. Gibson, R.K. Kremer, R.D. Hoffmann, R. Pöttgen, Unpublished results.
[49] K. Kadir, T. Sakai, I. Uehara, J. Alloys Compd. 287 (1999) 264.
[50] V.V. Kinzhibalo, A.T. Tyvanchuk, E.V. Melnik, R.M. Rychal, Visn. Lviv Univer. Ser. Chim. 29 (1988) 17.
[51] K. Kadir, H. Tanaka, T. Sakai, I. Uehara, J. Alloys Compd. 289 (1999) 66.
[52] K. Kadir, H. Yamamoto, T. Sakai, I. Uehara, N. Kanehisa, Y. Kai, L. Eriksson, Acta Crystallogr. C55 (1999) cifaccescode: IUC9900152.
[53] M.E. Kost, A.L. Shilov, N.T. Kuznetsov, Russ. J. Inorg. Chem. 33 (1988) 467.
[54] M.E. Drits, L.L. Rokhlin, N.P. Abrukina, V.V. Kinzhibalo, A.T. Tyvanchuk, Izv. Akad. Nauk SSSR, Metally (1985) 194.
[55] I.M. Opainich, V.V. Pavyluk, O.I. Bodak, Crystallogr. Rep. 41 (1996) 813.
[56] S. De Negri, M. Giovannini, A. Saccone, J. Alloys Compd. 427 (2006) 134.
[57] Z.M. Wang, H.Y. Zhou, T.F. Gu, G. Cheng, A.B. Yu, J. Alloys Compd. 381 (2004) 234.
[58] J.L. Sarrao, C.D. Immer, Z. Fisk, C.H. Booth, E. Figueroa, J.M. Lawrence, R. Modler, A.L. Cornelius, M.F. Hundley, G.K. Kwei, J.D. Thompson, F. Bridges, Phys. Rev. B 59 (1998) 6855.
[59] K. Aono, S. Orimo, H. Fujii, J. Alloys Compd. 309 (2000) L1.
[60] S. De Negri, M. Giovannini, A. Saccone, J. Alloys Compd. 427 (2007) 134.
[61] S. De Negri, M. Giovannini, A. Saccone, J. Alloys Compd. 397 (2005) 126.
[62] W. Rieger, H. Nowotny, F. Benesovsky, Monatsh. Chem. 95 (1964) 1502.
[63] J. Donohue, The Structures of the Elements, Wiley, New York, USA, 1974.
[64] N. Hanada, S.-I. Orimo, H. Fujii, J. Alloys Compd. 356–357 (2003) 429.
[65] M. Lukachuk, R. Pöttgen, Z. Kristallogr. 218 (2003) 767.
[66] F. Fourgeot, P. Gravereau, B. Chevalier, L. Fournès, J. Etourneau, J. Alloys Compd. 238 (1996) 102.
[67] P.I. Krypyakevich, V. Ya. Markiv, E.V. Melnyk, Dopov. Akad. Nauk. Ukr. RSR, Ser. A (1967) 750.
[68] A.E. Dwight, M.H. Mueller, R.A. Conner Jr., J.W. Downey, H. Knott, Trans. Met. Soc. AIME 242 (1968) 2075.
[69] M.F. Zumdick, R.-D. Hoffmann, R. Pöttgen, Z. Naturforsch. 54b (1999) 45.
[70] E. Parthé, L. Gelato, B. Chabot, M. Penzo, K. Cenzual, R. Gladyshevskii, TYPIX–standardized data and crystal chemical characterization of inorganic structure types. Gmelin Handbook of Inorganic and Organometallic Chemistry, 8th ed., Springer, Berlin, 1993.
[71] M.F. Zumdick, R. Pöttgen, Z. Kristallogr. 214 (1999) 90.
[72] W. Jeitschko, Acta Crystallogr. B 26 (1970) 815.
[73] R.-D. Hoffmann, R. Pöttgen, Z. Kristallogr. 216 (2001) 127.
[74] G. Nuspl, K. Polborn, J. Evers, G.A. Landrum, R. Hoffmann, Inorg. Chem. 35 (1996) 6922.
[75] G.A. Landrum, R. Hoffmann, J. Evers, H. Boysen, Inorg. Chem. 37 (1998) 5754.
[76] M.D. Bojin, R. Hoffmann, Helv. Chim. Acta 86 (2003) 1653.
[77] M.D. Bojin, R. Hoffmann, Helv. Chim. Acta 86 (2003) 1683.
[78] J. Gegner, T.C. Koethe, H. Wu, Z. Hu, H. Hartmann, T. Lorenz, T. Fickenscher, R. Pöttgen, L.H. Tjeng, Phys. Rev. B 74 (2006) 073102.
[79] G. Cordier, G. Dörsam, R. Kniep, J. Magn. Magn. Mater. 76–77 (1988) 653.
[80] R. Demchyna, Yu. Prots, U. Schwarz, Yu. Grin, Z. Anorg. Allg. Chem. 630 (2004) 1717.
[81] W. Choe, G.J. Miller, E.M. Levin, J. Alloys Compd. 329 (2001) 121.
[82] F. Canepa, M.L. Fornasini, F. Merlo, M. Napoletano, M. Pani, J. Alloys Compd. 312 (2000) 12.
[83] R. Kraft, R. Pöttgen, D. Kaczorowski, Chem. Mater. 15 (2003) 2998.
[84] R. Kraft, M. Valldor, R. Pöttgen, Z. Naturforsch. 58b (2003) 827.
[85] R. Kraft, M. Valldor, D. Kurowski, R.-D. Hoffmann, R. Pöttgen, Z. Naturforsch. 59b (2004) 513.
[86] R. Kraft, R. Pöttgen, Monatsh. Chem. 135 (2004) 1327.
[87] R. Kraft, R. Pöttgen, Z. Naturforsch. 60b (2005) 265.
[88] R. Kraft, R. Pöttgen, Monatsh. Chem. 136 (2005) 1707.
[89] B. Heying, R.-D. Hoffmann, R. Pöttgen, Z. Naturforsch. 60b (2005) 491.
[90] V.V. Karonik, D.N. Kazakov, R.A. Andrievskii, O.P. Bogachakova, Inorg. Mater. 20 (1984) 207.
[91] V.V. Karonik, D.N. Kazakov, R.A. Andrievskii, O.P. Bogachakova, Inorg. Mater. 20 (1984) 1416.
[92] R.-D. Hoffmann, U. Ch. Rodewald, R. Pöttgen, Z. Naturforsch. 54b (1999) 38.
[93] R. Pöttgen, M. Lukachuk, R.-D. Hoffmann, Z. Kristallogr. 221 (2006) 435.
[94] A. Doğan, D. Johrendt, R. Pöttgen, Z. Anorg. Allg. Chem. 631 (2005) 451.
[95] E.I. Gladyshevskii, P.I. Kripiakevich, M.J. Tesliuk, Dokl. AN SSSR 85 (1952) 81.
[96] K. Osamura, Y. Murakami, J. Less-Common Met. 60 (1978) 311.
[97] F.C. Frank, J.S. Kasper, Acta Crystallogr. 11 (1958) 184.
[98] F.C. Frank, J.S. Kasper, Acta Crystallogr. 12 (1959) 483.
[99] A. Simon, Angew. Chem. 95 (1983) 94.
[100] R. Nesper, Angew. Chem. 103 (1991) 805.
[101] R.L. Johnston, R. Hoffmann, Z. Anorg. Allg. Chem. 616 (1992) 105.
[102] R. Nesper, G.J. Miller, J. Alloys Compd. 197 (1993) 109.
[103] R. Zaremba, U. Ch. Rodewald, R. Pöttgen, Z. Kristallogr. Suppl. 24 (2006) 161.
[104] R. Zaremba, U. Ch. Rodewald, R.-D. Hoffmann, R. Pöttgen, Monatsh. Chem., in press.
[105] K. Kadir, T. Sakai, I. Uehara, J. Alloys Compd. 302 (2000) 112.
[106] D.T. Cromer, C.E. Olsen, Acta Crystallogr. 12 (1959) 689.
[107] D.E. Sands, A. Zalkin, O.H. Krikorian, Acta Crystallogr. 12 (1959) 461.
[108] E. Parthé, R. Lemaire, Acta Crystallogr. B 31 (1975) 1879.
[109] R. Ferro, R. Marazza, G. Rambaldi, A. Saccone, J. Less-Common Met. 40 (1975) 251.
[110] D.B. de Mooij, K.H.J. Buschow, J. Less-Common Met. 102 (1984) 113.
[111] A.E. Dwight, Mater. Res. Bull. 22 (1987) 201.
[112] K. Łątka, R. Kmieć, A.W. Pacyna, R. Mishra, R. Pöttgen, Solid State Sci. 3 (2001) 545.
[113] D. Johrendt, G. Kotzyba, H. Trill, B.D. Mosel, H. Eckert, Th. Fickenscher, R. Pöttgen, J. Solid State Chem. 164 (2002) 201.
[114] R. Mishra, R. Pöttgen, R.-D. Hoffmann, D. Kaczorowski, H. Piotrowski, P. Mayer, C. Rosenhahn, B.D. Mosel, Z. Anorg. Allg. Chem. 627 (2001) 1283.
[115] G. Kotzyba, R. Mishra, R. Pöttgen, Z. Naturforsch. 58b (2003) 497.
[116] T. Koyama, M. Matsumoto, T. Tanaka, H. Ishida, M. Mito, S. Wada, Phys. Rev. B 66 (2002) 014420.
[117] E. Figueroa, J.M. Lawrence, J.L. Sarrao, Z. Fisk, M.F. Hundley, J.D. Thompson, Solid State Commun. 106 (1998) 347.

[118] H. Sato, K. Hiraoka, M. Taniguchi, Y. Takeda, M. Arita, K. Shimada, H. Namatame, A. Kimura, K. Kojima, T. Muro, Y. Saitoh, A. Sekiyama, S. Suga, J. Synchrotron Radiat. 9 (2002) 229.
[119] J.M. Lawrence, P.S. Riseborough, C.H. Booth, J.L. Sarrao, J.D. Thompson, R. Osborn, Phys. Rev. B 63 (2001) 054427.
[120] H. Sato, K. Hiraoka, M. Taniguchi, Y. Nishikawa, F. Nagasaki, H. Fujino, Y. Takeda, M. Arita, K. Shimada, H. Namatame, A. Kimura, K. Kojima, J. Phys.: Condens. Matter 14 (2002) 4445.
[121] H. Hartmann, K. Berggold, S. Jodlauk, I. Klassen, K. Kordonis, T. Fickenscher, R. Pöttgen, A. Freimuth, T. Lorenz, J. Phys.: Condens. Matter 17 (2005) 7731.
[122] L.J. Huang, G.Y. Liang, Z.B. Sun, Y.F. Zhou, J. Alloys Compd. 432 (2007) 172.
[123] Z.M. Wang, H.Y. Zhou, G. Cheng, Z.F. Gu, A.B. Yu, J. Alloys Compd. 384 (2004) 279.
[124] Z.M. Wang, H.Y. Zhou, Z.F. Gu, G. Cheng, A.B. Yu, J. Alloys Compd. 377 (2004) L7.
[125] L.Z. Ouyang, F.X. Qin, M. Zhu, Scr. Mater. 55 (2006) 1075.
[126] Q. Li, K.-D. Xu, K.-Ch. Chou, X.-G. Lu, J.-Y. Zhang, G.-W. Lin, Intermetallics 15 (2007) 61.
[127] K. Tanaka, J. Alloys Compd., in press.
[128] L. Gao, Ch. Chen, L. Chen, Q. Wang, Ch. Wang, Y. An, J. Alloys Compd. 424 (2006) 338.
[129] Q. Li, X.-G. Lu, K.-Ch. Chou, K.-D. Xu, J.-Y. Zhang, S.-L. Chen, Int. J. Hydrogen Energy, in press.
[130] F. Zhang, Y. Luo, A. Deng, Zh. Tang, L. Kang, J. Chen, Electrochim. Acta 52 (2006) 24.
[131] D. Wang, Y. Luo, R. Yan, F. Zhang, L. Kang, J. Alloys Compd. 413 (2006) 193.
[132] S. Zhang, H. Zhou, Zh. Wang, R.P. Zou, H. Xu, J. Alloys Compd. 398 (2005) 269.
[133] X. Xu, H.Y. Zhou, R.P. Zhou, S.L. Zhang, Z.M. Wang, J. Alloys Compd. 396 (2005) 247.
[134] Q. Li, K.-Ch. Chou, K.-D. Xu, Q. Lin, L.-J. Jiang, F. Zhan, J. Alloys Compd. 387 (2005) 86.
[135] H.G. Pan, Y.F. Liu, M.X. Gao, R. Li, Y.Q. Lei, Intermetallics 13 (2005) 770.
[136] B. Liao, Y.Q. Lei, G.L. Lu, L.X. Chen, H.G. Pan, Q.D. Wang, J. Alloys Compd. 356–357 (2003) 746.
[137] Y.-H. Zhang, X.-P. Dong, S.-H. Guo, G.-Q. Wang, J.-Y. Ren, X.-L. Wang, J. Alloys Compd. 398 (2005) 178.
[138] T. Kohno, H. Yoshida, F. Kawashima, T. Inaba, I. Sakai, M. Yamamoto, M. Kanda, J. Alloys Compd. 311 (2000) L5.
[139] F.-L. Zhang, Y.-Ch. Luo, J.-P. Chen, R.-X. Yan, J.-H. Chen, J. Alloys Compd. 430 (2007) 302.
[140] F. Zhang, Y. Luo, K. Sun, D. Wang, R. Yan, L. Kang, J. Chen, J. Alloys Compd. 424 (2006) 218.
[141] L. Guénée, K. Yvon, J. Alloys Compd. 356–357 (2003) 114.
[142] J.-L. Bobet, P. Lesportes, J.-G. Roquefere, B. Chevalier, K. Asano, K. Sakai, E. Akiba, Int. J. Hydrogen Energy, in press.
[143] J.-N. Chotard, Ya. Filinchuk, B. Revaz, K. Yvon, Angew. Chem. Int. Ed. 45 (2006) 7770.
[144] K. Yvon, G. Renaudin, C.M. Wei, M.Y. Chou, Phys. Rev. Lett. 94 (2005) 066403.
[145] B. Huang, K. Yvon, P. Fischer, J. Alloys Compd. 197 (1993) 65.
[146] B. Huang, K. Yvon, P. Fischer, J. Alloys Compd. 227 (1995) 116.
[147] K. Schubert, K. Anderko, Z. Metallkd. 42 (1951) 321.
[148] J. Schefer, P. Fischer, W. Hälg, F. Stucki, L. Schlapbach, J.J. Didisheim, K. Yvon, A.F. Andresen, J. Less-Common Met. 74 (1980) 65.
[149] D. Noréus, P.-E. Werner, Acta Chem. Scand. A 36 (1982) 847.
[150] V. Hlukhyy, U. Ch. Rodewald, R. Pöttgen, Z. Anorg. Allg. Chem. 631 (2005) 2997.
[151] Q. Li, K.C. Chou, Q. Lin, Int. J. Hydrogen Energy 29 (2004) 843.
[152] A. Inoue, A. Kato, T. Zhang, S.G. Kim, T. Masumoto, Mater. Trans. JIM 33 (1992) 937.
[153] S.S. Wu, T.S. Chin, K.C. Su, Int. J. Rapid Solid. 8 (1993) 65.
[154] A. Inoue, T. Masumoto, Mater. Sci. Eng. A 173 (1993) 1.
[155] C.H. Kam, Y. Li, S.C. Ng, A. Wee, J.S. Pan, H. Jones, J. Mater. Res. 14 (1999) 1638.
[156] A. Gebert, U. Wolff, A. John, J. Eckert, L. Schultz, Mater. Sci. Eng. A. 299 (2001) 125.
[157] M. Savyak, S. Hirnyj, H.-D. Bauer, M. Uhlemann, J. Eckert, L. Schultz, A. Gebert, J. Alloys Compd. 364 (2004) 229.